AN EXPERIMENTAL STUDY OF UPWARD AND DOWNWARD FLOW OF SUPERCRITICAL CARBON DIOXIDE IN A STRAIGHT PIPE HEAT EXCHANGER WITH CONSTANT WALL HEAT FLUX

A Thesis

by

ERIC DARA UMRIGAR

Submitted to the Office of Graduate and Professional Studies of
Texas A&M University
in partial fulfillment of the requirements for the degree of

MASTER OF SCIENCE

Chair of Committee,	Devesh Ranjan
Committee Members,	Kalyan Annamalai
	Karen Vierow
Head of Department,	Andreas A. Polycarpou

May 2014

Major Subject: Mechanical Engineering

ABSTRACT

An experimental analysis was conducted on a single circular tube heat exchanger using supercritical carbon dioxide as the working fluid. The heat exchanger was operated in two different orientations: vertically upward and downward. The experimental facility utilized two different mass flow rates: a low flow rate of 0.0183 kg/s and a high mass flow rate 0.03 kg/s, three system pressures: 7.5, 8.1 and 10.2 MPa and two different heat inputs: a low heat input of 540 W and a high heat input of 955 W. Inlet temperatures to the test section were varied from 20-55°C. Thermocouples on the surface of the test section recorded the wall temperatures. Then, a one dimensional heat transfer analysis was conducted to calculate inner wall temperatures. Afterwards, the bulk temperature was calculated using a constant heat flux approximation and an energy balance on a differential control volume. Finally, the local heat transfer coefficient between the bulk and inner wall was calculated.

Results showed that typically, for the 7.5 and 8.1 MPa cases, as the temperature reached the pseudocritical point, there was a heat transfer deterioration followed immediately by a substantially large heat transfer enhancement. After the critical temperature was reached, however, the heat transfer coefficient decreased. The results showed that the heat transfer coefficient, deterioration and enhancement were the greatest with the 7.5 MPa case and the downward orientation. Buoyancy effects seem to be present and have a significant impact on the heat transfer coefficient.

In general, if heat exchangers are to be designed to be used with supercritical fluids, they should be designed, along with other important components, to be operated as close to the critical point as possible as well as have a downward flowing orientation to maximize heat transfer potential.

DEDICATION

I would like to dedicate this thesis to my mother, Vira and my father Dara. With their love and support, this work was made possible.

I also dedicate this thesis to my friends who have helped me along my path in college to help make this work possible.

ACKNOWLEDGEMENTS

I would like to give thanks to my committee chair, Dr. Devesh Ranjan and my committee members, Dr. Kaylan Annamalai and Dr. Karen Vierow for their support and mentorship throughout this research. I know all of you have taken a lot of time out of your busy days to give me assistance on this research.

I would also like give special thanks to my colleagues Jacob McFarland, Sandeep Pidaparti, and Bryce Matsuo. These individual have taken a considerable portion of their time to help me on this research. Thanks to all my other colleagues as well. It was with their assistance and guidance that this research was possible.

NOMENCLATURE

A	Area [m^2]
c_p	Specific Heat [kJ/kg-K]
d	Diameter [m]
d_h	Hydraulic Diameter [m]
H	Heat Transfer Coefficient [W/m^2-K]
h	Enthalpy [kJ/kg]
k	Thermal Conductivity [W/m-K]
$\dot{m}$	Mass Flow Rate [kg/s]
N_u	Nusselt Number [-]
P	Pressure [MPa]
Pr	Prandtl Number [-]
Re	Reynolds Number [-]
T	Temperature [°C]
t	Time [s]
v	Specific Volume [m^3/kg]
W	Work [kJ]

Greek Symbol

ρ	Density [kg/m^3]

Subscripts

b	Bulk Property
c	Critical
pc	Pseudo critical
t	Turbulent
w	At Wall Property
JH	Jackson-Hall

TABLE OF CONTENTS

Page

LIST OF FIGURES

Page

LIST OF TABLES

Page

CHAPTER I

INTRODUCTION

As technology progresses and the world population continues to increase, the demand for energy will only increase. New sources for energy are constantly being sought. As a result, alternative energy sources have been given particular attention. The three most common sources of alternative energy are solar, wind and nuclear energy. Lately, special attention is given to nuclear energy.

If all goes according to plan, in 2030, the Generation IV Nuclear Reactors will go online [1]. There have been several proposed reactor concepts for the reactor design. One of the proposed cycles to be used is a supercritical carbon dioxide Brayton cycle. In this cycle, a conventional Brayton cycle, as shown in Figure 1, is modified such that the combustion chamber is replaced with a heat exchanger.

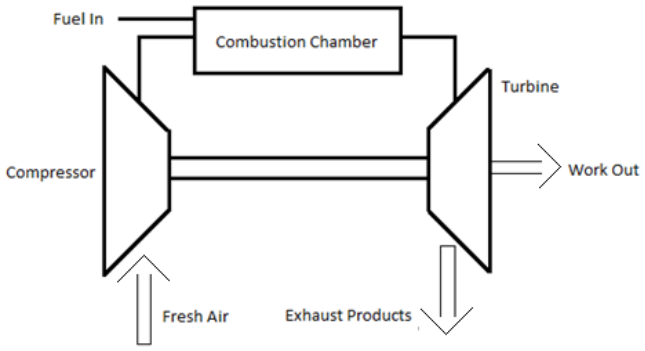

Figure 1: The Standard Brayton Cycle

The heat exchanger essentially has the same function as the combustion chamber, to increase temperature and thus, pressure of the working fluid. Figure 2 below shows a simplified carbon dioxide Brayton cycle. Since the carbon dioxide is not consumed during the cycle operation, a closed loop Brayton cycle can be employed. The expanded gases through the turbine are then cooled upon exiting in another heat exchanger to increase the density of the carbon dioxide before being sent to the compressor again.

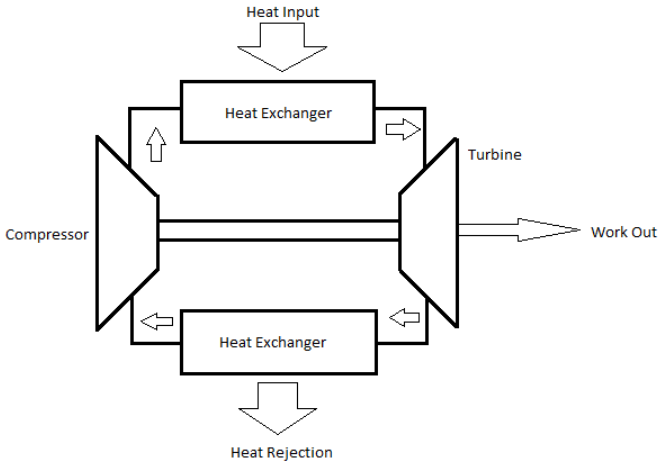

Figure 2: Simplified Carbon Dioxide Brayton Cycle

In order to increase the thermal efficiency of the cycle, the waste heat from the exhaust products should be recovered. Printed circuit heat exchangers (PCHE), as studied by Bryce Matsuo among many other researchers, can be placed between the exhaust of the turbine and the inlet of the thermal energy input heat exchanger [2]. This type of heat exchanger is very compact, often only a small fraction of the size of a

typical heat exchanger. Figure 3 below shows the closed loop Brayton cycle with a printed circuit heat exchanger.

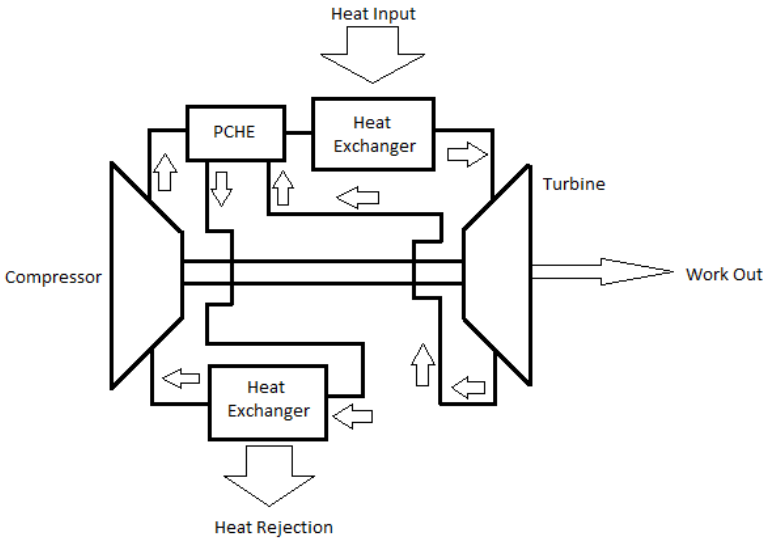

Figure 3: Supercritical Carbon Dioxide Brayton Cycle with Printed Circuit Heat Exchanger

Printed circuit heat exchangers are constructed from flat pieces of bar stock, typically from stainless steel. Then, a chemical etching process is conducted where certain patterns are chemically etched onto the surface of the bar stock. The etched patterns can be of almost any design. The most commonly studied are the s-shaped channels, zigzag channels and airfoil channels. These geometries can be seen below in Figure 4.

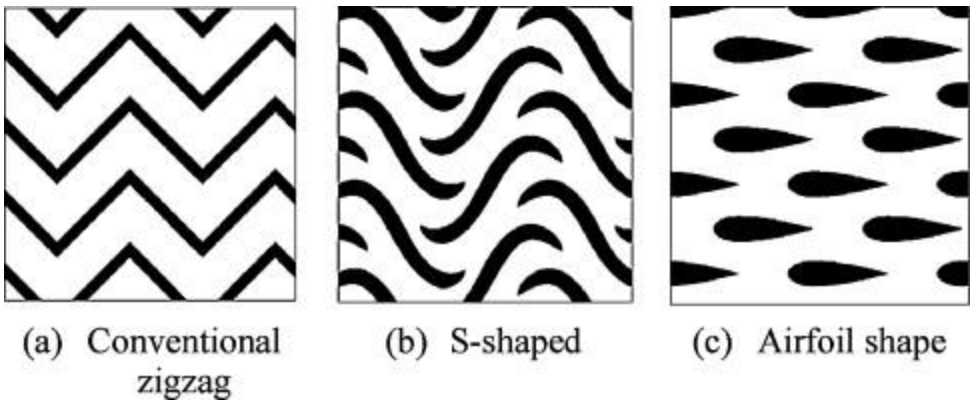

Figure 4: PCHE Studied Geometries (Image taken from [3])

It was found through previous research that the conventional zigzag channel PCHE has arguable one of the best heat transfer performance. However, the zigzag channel also has the largest pressure drop across it. An s-shaped geometry was also studied. This geometry gave heat transfer performance similar to the zigzag channel but with about one-fifth the pressure drop of the zigzag channel. Finally, an airfoil shape PCHE was analyzed. The airfoil PCHE had lower overall heat transfer coefficients compared to the zigzag channel but also the smallest pressure drop, about one-twentieth of the zigzag channel [3]. Different geometries will be continually developed and studied in an effort to maximize heat transfer and reduce pressure drops.

Review of Supercritical Fluids

All fluids possess a supercritical phase. A fluid that is in the supercritical phase is essentially a fluid that is above its critical temperature and pressure. It is a state where

the fluid is not truly a pure liquid or a pure vapor. The distinction between the two phases simply disappears. In the supercritical state, fluids possess liquid-like densities and vapor-like viscosities. Looking at the temperature-entropy diagram, shown in Figure 5, the critical point is located where the lines of saturated liquid and saturated vapor meet.

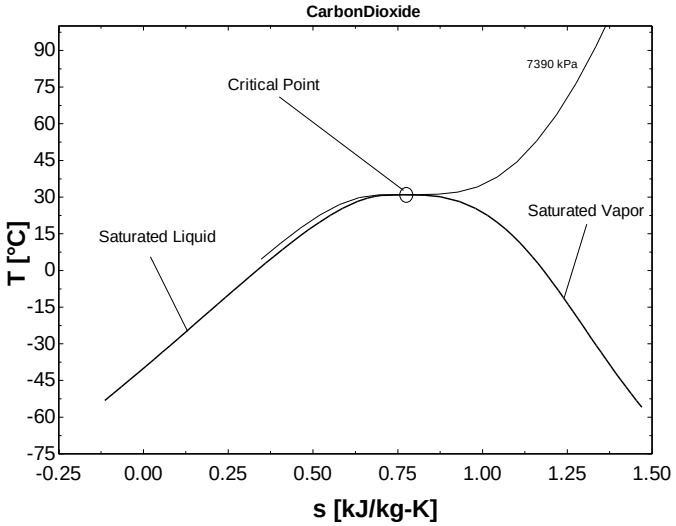

Figure 5: T-s Diagram for Carbon Dioxide [4]

Figure 5 also shows that the critical point of carbon dioxide is about 31.1℃ at 7.38 MPa. At the critical point, fluids can exhibit drastic property fluctuations. Even though the properties may fluctuate at or above the critical point, the fluid still remains in a single phase. The critical point for any substance is defined as follows:

$$\left(\frac{\partial P}{\partial v}\right)_T = 0 \qquad (1)$$

In words, the critical point can be defined as saying that the change in pressure with respect to the change in volume is zero at constant temperature. In other words, no matter how much the volume changes, the pressure will remain constant at that given temperature. If the pressure and temperature are above the critical point, for any given temperature there exists a pseudocritical point. The effects of property fluctuations described previously are not as pronounced with pseudocritical point as they are with the critical point. According to Liao and Zhao, the pseudocritical temperature of carbon dioxide can be found using the following equation [5]:

$$T_{pc} = -122.6 + 6.124p - 0.1657p^2 + 0.01773p^{2.5} - 0.0005608p^3 \quad (2)$$

where the pressure, p, is in bar. Table 1 below shows the pseudocritical temperatures for the system pressures used in this thesis.

Table 1: Pseudocritical Temperature of Carbon Dioxide at Various Pressures

Pressure	Pseudocritical Temperature
7.5 MPa	32.05 °C
8.1 MPa	35.49 °C
10.2 MPa	46.26 °C

Figure 6 below shows the drastic changes in density of various pressures at their corresponding critical points.

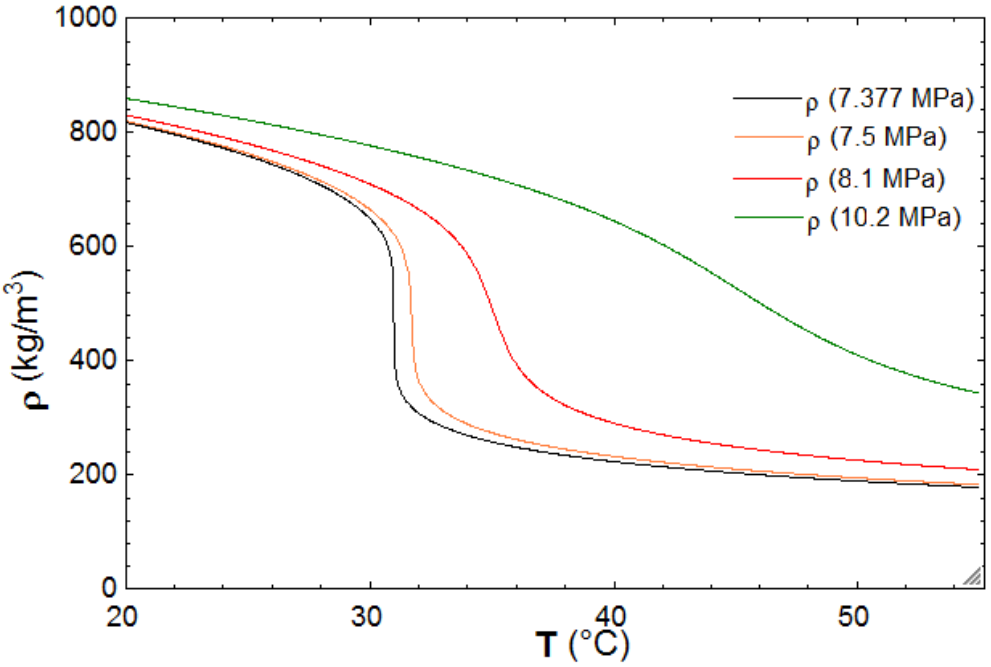

Figure 6: Density of Carbon Dioxide at Various Pressures [4]

There is a drastic decrease in the densities at the critical point. It is also important to note that as pressures increases, the peak density values increase as expected.

Figure 7 shows the corresponding trend of specific heat. The behavior of specific heat is nearly the opposite of density. At the critical point, there is a sharp rise in the specific heat. Theoretically, the specific heat reaches infinity at the critical point. At this point, heat transfer potential of the fluid is the greatest.

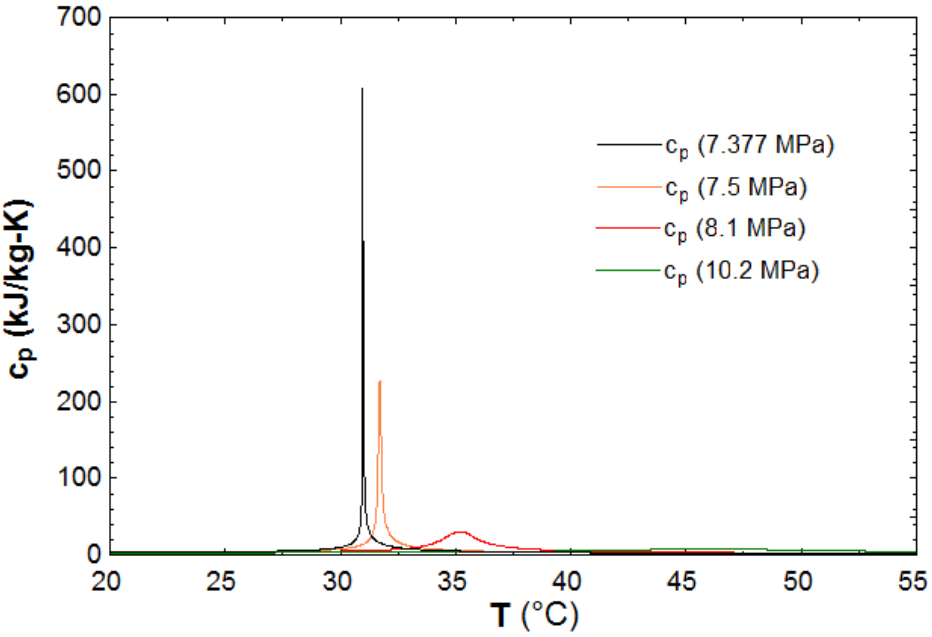

Figure 7: Specific Heat of Carbon Dioxide at Various Pressures [4]

Figure 8 shows the thermal conductivity of carbon dioxide at the various pressures. Again, at the critical point, a sharp rise occurs. This suggests that the thermal conductivity is at a maximum at the critical point. The peak of the conductivity at the critical point will play a crucial role in the development of heat exchangers that utilize supercritical fluids.

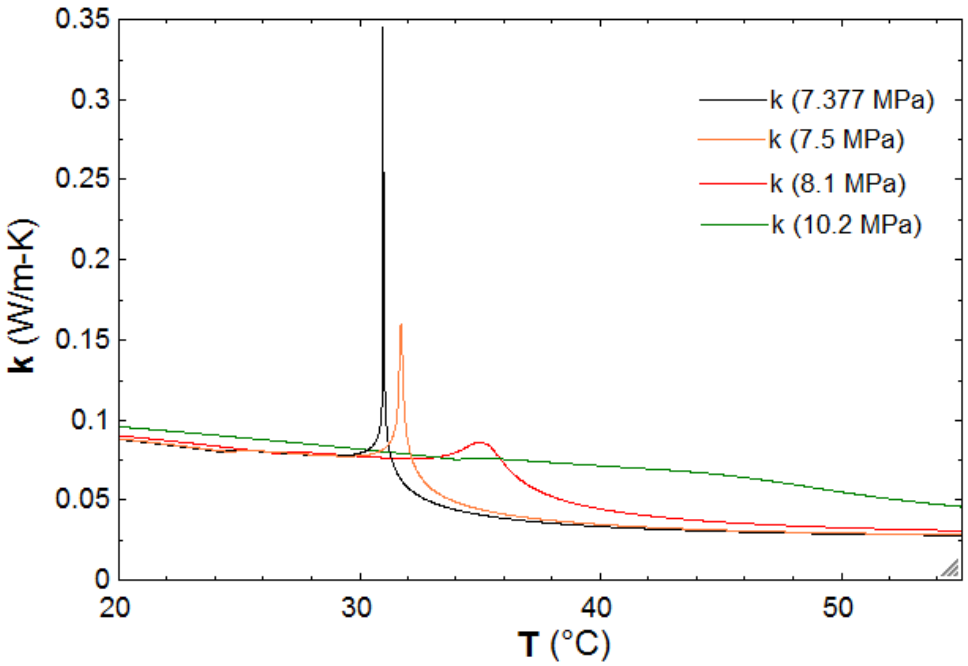

Figure 8: Thermal Conductivity of Carbon Dioxide at Various [4]

Essentially, all of the preceding property figures show that when designing a heat exchanging system to be used with a supercritical fluid, the critical or pseudocritical points should be thoroughly investigated and exploited for maximum system performance.

Motivation

The motivators for this experiment were numerous. First, the components used in a supercritical carbon dioxide Brayton Cycle can be made much smaller in physical size compared to standard steam cycle components. One reason for this is the very high density of carbon dioxide at the proposed turbine inlet conditions of 550 °C and about

2900 psi [6]. The density of carbon dioxide at these conditions is about 125 kg/m^3 [7]. On the other hand, the density of steam is roughly 52 kg/m^3 at typical Rankine cycle operating conditions of about 538 °C and 2525 psi [8]. Figure 9 below shows a scaled size comparison of supercritical carbon dioxide system components to steam and helium cycle components as presented by Sandia National Laboratories [9].

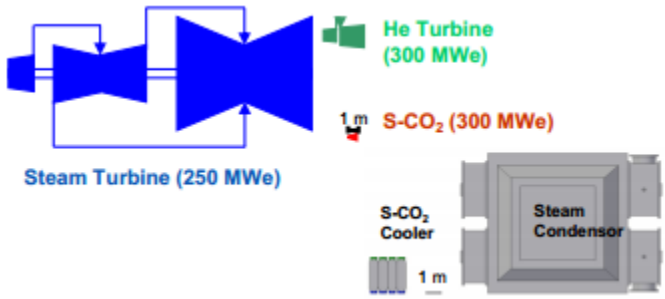

Figure 9: Comparison of S-CO_2 system components to Steam and Helium Cycle Components (Image taken from [9])

As one can see, the system components can be made significantly smaller than their steam or helium cycle counterparts. This allows for a very high energy per unit volume displaced ratio. In other words, power plants utilizing this technology can be made smaller and therefore have reduced start up costs.

Secondly, as mentioned earlier, there are no phase changes in a supercritical carbon dioxide cycle. The fluid remains completely in the supercritical phase. Traditional components such as condensers are not required in these advanced cycles. A single phase cycle also eliminates the potential of cavitation in the pumps in a system. This would extend the life of the components. Also, carbon dioxide has one of the

easiest attainable critical points compared to its main competitors, water and helium. Table 2 below shows the critical points for these fluids.

Table 2: Critical Points of Carbon Dioxide, Water and Helium

Substance	Critical Temperature	Critical Pressure
Carbon Dioxide	31.1 °C	7.38 MPa
Water	374.1 °C	22.11 MPa
Helium	-267.96 °C	0.23 MPa

Water requires a significantly higher temperature and pressure to be in the supercritical state, while helium requires a low pressure but also a very low temperature. Although this may make helium sound to be the better choice, it is important to remember that the operating conditions for the helium cycle will be much further away from the critical point.

Finally, in a supercritical Brayton cycle there is less compressor work required compared to its main competitor, the helium Brayton Cycle. This is primarily due to the lower density of the carbon dioxide under the operating conditions of the proposed supercritical Brayton cycle. According to Dostal *et al.* the compressor in the helium Brayton cycle will consume about 45% of the turbine output compared to about 30% with supercritical carbon dioxide Brayton cycle [10]. This also allows for the use of a single compressor without intercooling, thus, this further reduces costs compared to the helium Brayton cycle [10].

Organization

The previous chapter gave an overview of supercritical fluids and the motivation behind why the research in this thesis was necessary. It also gave an in depth review of the behavior of supercritical fluids.

Chapter 2 of the thesis will provide a literature review of some of the research that has been accomplished in this field. This chapter will show the works of a few of the researchers that have had a prominent impact on supercritical fluids. The content of this chapter will also be used a basis for the further research required in this field that was accomplished in this thesis. Furthermore, some of the data reduction methods used by two prominent researchers, Kim *et al.* and Kruizenga *et al.*, will be examined in depth. This further examination was important because, this thesis uses a slightly different data reduction method than what has previously been used.

Chapter 3 will describe the experimental setup in rigorous detail. This chapter will talk about the specifications about each major component and why that component was chosen for this experimental facility.

Chapter 4 will show the data reduction method used for this thesis and how it differs from the reduction method of previous researchers. This chapter will also show the steps taken to validate the experimental facility.

Chapter 5 will show and discuss the experimental results. Furthermore, a test matrix will be provided that shows the combination of variables that were altered in

order to see the effects those variables would have on the heat transfer. The results will be presented in a series of plots and charts. The behavior of the supercritical carbon dioxide for each individual case will be analyzed. Also error bars for each of the data sets will be presented to factor in the total error on each measurement taken.

Chapter 6 will present the conclusions of this thesis. All of the major findings will be summarized in this chapter.

Finally, Chapter 7 will present a future works section. The future work section will discuss the changes that will be applied to the experimental facility used for this thesis to carry on the research to the next level.

CHAPTER II

LITERATURE REVIEW

The main purpose of this section is to show some of the important studies that have been conducted in the field of supercritical fluids. In turn, the previous research will be used as a basis in this thesis to show how the research in this thesis provides a path that will hopefully provide a deeper understanding of supercritical carbon dioxide. This section begins by examining thoroughly the works of two researchers, Kim *et al.* and Kruizenga *et al.*, due to them conducting very similar experiments to those conducted in this thesis. Afterwards, the works of some of the other pertinent researches will be briefly analyzed.

Work of Prominent Researchers

In 1999, at the K.N. Toosi University of Technology in Tehran, Iran, Majid Bazargan and Mahdi Mohseni conducted a numerical study to analyze the convection heat transfer deterioration due to the variations of Eddy viscosity and the fluid properties of supercritical fluids. Their results showed that when the flow turbulence is suppressed, the heat transfer deterioration can be partly caused by the decrease of the turbulent viscosity [11]. Bazargan and Mohseni's findings are significant because prior to their investigation, it was believed that buoyancy and thermal acceleration effects were the two main mechanisms for heat transfer deterioration [11].

In 2005, Vaclav Dostal *et al*. conducted computational research to investigate how a supercritical carbon dioxide Brayton cycle compares with a supercritical helium Brayton cycle with multiple compressors [6]. Through their research, it was found that the multi-state helium cycle was more efficient at the expense of more equipment capital and larger system size. Dostal *et al.* also noted that the supercritical carbon dioxide cycle operates at a much lower peak temperature than the supercritical helium cycle, 550°C vs. 880°C, respectfully [6].

Supercritical carbon dioxide has also been considered for a refrigerant in air conditioning units in automobiles. If supercritical carbon dioxide is used as a refrigerant, the high pressure side of an air conditioning system changes from a condensation process to a supercritical gas cooling process. In 2002, Srinivas S. Pitla *et al.* studied the supercritical carbon dioxide for use in a tube in tube heat exchanger for possible use as a working fluid in an automotive air conditioning unit. Through their research, they were able to develop a new correlation to compute the Nusselt number in terms of other dimensionless parameters. This equation is shown below:

$$Nu = \left(\frac{Nu_{wall} + Nu_{bulk}}{2}\right)\frac{k_{wall}}{k_{bulk}} \tag{3}$$

where Nu_{wall} and Nu_{bulk} are the Nusselt numbers that are evaluated at the wall and bulk temperatures, respectfully, and k_{wall} and k_{bulk} are the thermal conductivities evaluated at

the wall and bulk temperatures [12]. The wall and bulk Nusselt numbers were calculated using the Gnielinski correlation [13] as shown below:

$$Nu = \frac{\xi/8(Re - 1000)Pr}{12.7\sqrt{\frac{\xi}{8}}\left(Pr^{\frac{2}{3}} - 1\right) + 1.07} \quad (4)$$

Pitla *et al.* acknowledged that there were very few attempts made prior to their research on the subject of in-tube cooling of carbon dioxide. Various other researcher such as Petrov and Popov [14], Baskov *et al.* [15]and Krasnoshechekov [16] attempted to find a correlation for the heat transfer in supercritical carbon dioxide during cooling mode. Their correlations were too complex and didn't particularly predict the data well in the pseudocritical region[12].

Then in 2008, Cheng *et al.* analyzed the cooling behavior of supercritical carbon dioxide in macro-channels as well as micro-channels. They concluded that for a given pressure, in cooling mode, the heat transfer coefficient will increase to maximum with decreasing temperatures [17]. The maximum occurs near the pseudocritical temperature. Also, they found that the tube diameter has little affect on the heat transfer coefficient when the temperature of the carbon dioxide is less than the pseudocritical temperature [17].

In 2010, Yoon Y. Bae conducted experiments on the heat transfer to carbon dioxide in an upward and downward flowing vertical tube and an annular channel. From

the conducted experiments, Bae concluded several things. First, the heat transfer in an upward flowing tube decreased as the wall heat flux was increased. This trend continued to a point after which heat transfer rate deteriorated [18]. Second, the heat transfer rates in the tube as well as the annular channel were nearly identical for the same specified test conditions. The heat transfer rates in the annular channel were slightly lower than the vertical tube [18]. Finally, heat transfer deterioration was observed in both the upward and downward cases. However, it was noted that in the downward cases, the magnitude of the deterioration was lower [18].

In addition to research being carried out in single channels, there has been countless research on printed circuit heat exchangers. In 2012, Matt Carlson *et al*. conducted research on the heat transfer and pressure drop of supercritical carbon dioxide flowing in various printed circuit heat exchanger designs. They conducted experiments on two designs, an 80-degree bend zig-zag channel and 8.1mm NACA 0020 airfoil shaped staggered pillar array [19]. Carlson *et al.* concluded that existing correlations for piping network can be used to sufficiently predict the hydraulic performance of the zig-zag channel heat exchanger and the asymptotic behavior of the airfoil heat exchanger [19]. They also suggest that the existing correlations can be used to design various other printed circuit heat exchangers geometries. Lastly, Carlson *et al.* found that the performance of both heat exchanger designs was about 2 to 2.5 times under predicted by Jackson's [20] correlation [19].

Work of Kim et al.

In this section, the work of Hwan Yeol Kim *et al.* will be examined in rigorous detail. The reasoning behind this is that the setup of Kim et al. is similar to the setup used in this thesis.

Kim *et al.* studied the heat transfer of carbon dioxide in a vertical tube at supercritical pressures [21]. Their heat transfer facility, called Supercritical Pressure Heat Transfer Investigation of NeXt Generation, or SPHINX, was constructed at the Korea Atomic Energy Research Institute, or KAERI, in 2007 [21]. The layout of their experimental facility can be described in the following manner. Carbon dioxide is supplied from a tank and its pressure is increased using a separate pump. Kim *et al.* used an air driven pump to increase the pressure. A gear type pump was used to circulate the fluid throughout the system. The test section was heated using electric resistive heating. An electric preheater was used to control the inlet temperature of the test section and a chiller unit was used to cool down the carbon dioxide once it has passed through the test section.

Kim *et al.* used 20 mm inner diameter tubing for the loop excluding the test section and 4.4 mm inner diameter tubing for the test section. The 4.4 mm tubing was sized for a Reynolds's number of about 50000. They fixed the inlet test section temperature to 27 °C. The inlet pressures used were 7.75, 8.12 and 8.85 MPa. The surface heat flux was 150 kW/m^2. They used a range of mass fluxes from 400-1200 kg/m^2s.

Kim *et al.* reduced their data in the following manner. They began by first, calculating the heat flux that entered the test section that was transferred to the fluid by the following relationship:

$$q^{"} = \frac{\dot{Q}}{(\pi D_i L_h)} = \frac{V_{PSU} I_{PSU}}{\pi D_i L_h} \tag{5}$$

where $\dot{Q}$, is the heat transfer rate, D_i is the inner diameter, L_h is the length of the tube, V and I are the voltage and current of the power supply unit (PSU) respectively. Numerous thermocouples were mounted to the surface of the test section. To determine the inner wall temperatures, a simple one-directional heat transfer was assumed. The following equation describes how the inner wall temperature was calculated:

$$T_{w,i} = T_{w,o} + \frac{\dot{q}}{4k_w}\left[\left(\frac{D_o}{2}\right)^2 - \left(\frac{D_i}{2}\right)^2\right] - \frac{\dot{q}}{2k_w}\left(\frac{D_o}{2}\right)^2 ln\frac{D_o}{D_i} \tag{6}$$

where, $T_{w,i}$ is the inner wall temperature, $T_{w,o}$ is the outer wall temperature, D_o and D_i represent the outer and inner diameters, respectively and $\dot{q}$ is the volumetric generation rate.

They found that the Dittus-Boelter correlation typically over predicted the heat transfer coefficients near the pseudo-critical temperatures. This correlation did, however, predict the heat transfer coefficient well in the temperature ranges away from the pseudo-critical temperatures since the fluid behaves as a single phase fluid.

It was also observed that at mass fluxes of 400 and 500 kg/m^2, there was heat transfer deterioration if the input heat flux is greater than 40 kW/m^2 for the 400 kg/m^2 flux case and about 50 kW/m^2 for the 500 kg/m^2 flux case. Heat transfer deterioration was also observed with the 750 kg/m^2 case at input heat fluxes of 90kW/m^2. Heat transfer deteriorations were not observed in the 1000 and 1200 kg/m^2 flux cases. That finding showed that as mass flux was increased, the deterioration decreased.

Finally, Kim *et al.* compared their obtained results with well know heat transfer correlations. A brief listing of the correlations is shown below in Table 3.

Table 3: Correlations of Various Prominent Supercritical Fluid Researchers

Krasnoshchekov and Protopopov	$$Nu = \frac{hD}{k_b} = Nu_o \left(\frac{\rho_w}{\rho_b}\right)^{0.3} \left(\frac{\bar{c_p}}{c_{pb}}\right)^n$$ $$where\ n$$ $$= \begin{cases} 0.4\ for\ T_b < T_w < T_{pc}\ and\ 1.2 * T_{pc} < T_b < T_w \\ 0.4 + 0.2\left[\left(\frac{T_w}{T_{pc}}\right) - 1\right]\ for\ T_b < T_{pc} < T_w \\ 0.4 + 0.2\left[\left(\frac{T_w}{T_{pc}}\right) - 1\right]\left\{1 - \left[5\left(\frac{T_b}{T_{pc}}\right) - 1\right]\right\} \\ for\ T_{pc} < T_b < 1.2T_{pc}\ and\ T_b < T_w \end{cases}$$ $$Nu_o = \frac{\left(\frac{\xi}{8Re_bPr_b}\right)}{12.7\sqrt{(\xi/8)}\left(Pr_b^{2/3}\right) + 1.07}$$ $$where: Re_b = \frac{GD}{\mu_b}, Pr_b = \frac{c_{pb}\mu_b}{k_b}, \overline{c_{pb}} = \frac{i_w - i_b}{T_w - T_b},$$ $$\xi = (1.82logRe_b - 1.64)^{-2}$$

Table 3: Continued

Modified Krasnoshchekov and Protopopov	$Nu = \frac{hD}{k_b} = 0.0183 Re_b^{0.82} Pr_b^{0.5} \left(\frac{\rho_w}{\rho_b}\right)^{0.3} \left(\frac{\bar{c_p}}{c_{pb}}\right)^n$ $where\ n\ is\ the\ same\ as$ Krasnoshchekov and Protopopov
Jackson and Fewster	$Nu = \frac{hD}{k_b} = 0.0183 Re_b^{0.82} \overline{Pr_b}^{0.5} \left(\frac{\rho_w}{\rho_b}\right)^{0.3}$; $\overline{Pr_b} = \frac{\bar{c_p}\mu_b}{k_b}$
Watts and Chou	$\frac{Nu}{Nu_{var\ p}}$ $= \begin{cases} \left[1 - 3000 \frac{\overline{Gr_b}}{Re_b^{2.7} \overline{Pr^{0.5}}}\right]^{0.295} & for\ \frac{\overline{Gr_b}}{Re_b^{2.7} \overline{Pr_b^{0.5}}} < 10^{-4} \\ \left[7000 \frac{\overline{Gr_b}}{Re_b^{2.7} \overline{Pr_b}^{0.5}} \geq 10^{-4}\right]^{0.295} & for\ \frac{\overline{Gr_b}}{Re_b^{2.7} \overline{Pr_b^{0.5}}} < 10^{-4} \end{cases}$ $where\ Nu_{var\ p} = 0.021 Re_b^{0.8} \overline{Pr_b}^{0.55} \left(\frac{\rho_w}{\rho_b}\right)^{0.35}$ $\overline{Gr_b} = \frac{\rho_b(\rho_b - \rho_m) g D^3}{\mu_b^2}\ and\ \rho_m = \frac{1}{T_w - T_b} \int_{T_b}^{T_w} \rho dT$

Kim *et al.* showed that the Jackson [20] correlation predicted the behavior the best compared to the other correlations in the supercritical region in terms of the maximum standard deviation. However, all of the correlations seemed to predict the behavior with about the same error.

Work of Kruizenga et al.

Next, the work of Alan Kruizenga *et al.* was analyzed for essentially the same reasons as the work of Kim *et al.* [22]. In 2011, they researched the heat transfer of supercritical carbon dioxide in various heat exchanger geometries. Their experimental set up consisted of several key components. First, the main circulation pump, the ChemPump, circulated the fluid throughout the loop after the system had been charged to the desired pressure level using the high performance liquid chromatography (HPLC) pump. A Coriolis flow meter was used to measure the flow rate and a preheater was used to ensure proper test section inlet temperatures. A throttle valve was used to fine tune the pressure of the system. Finally, a chilled water recirculation loop was used to cool the carbon dioxide before it entered the ChemPump to repeat the process. The test section consisted of a semi-circular straight channel printed circuit heat exchanger encased in a cooling jacket. Thermocouples were probed into the heat exchanger.

The data obtained from their experiment was reduced in the following manner. During the cooling process, heat was transferred into the water from the carbon dioxide. The amount of heat absorbed and removed was calculated using equations 7 and 8 respectfully.

$$Q_{H_2O} = \sum_{i=1}^{20} \dot{v}_i \rho_i C_{p-i} \left(T_{1-i} - T_{2-i}\right) \tag{7}$$

$$Q_{CO_2} = \dot{m}(i_{in} - i_{out}) \tag{8}$$

Afterwards, Kruizenga *et al.* conducted an energy balance on the test section to calculate the outlet enthalpy, i, of the carbon dioxide. The energy balance is shown in the equation below.

$$i_{CO_2}[j+1] = i_{CO_2}[j] - \frac{Q_j}{\dot{m}} \tag{9}$$

Using the energy balance and knowing the temperature at j+1, the bulk temperature became a known quantity. Next, the local inner wall temperatures were calculated as follows:

$$T_w[j] = 0.5(T_{top}[j] + \frac{q_{top}[j]z}{kA} + T_{bottom}[j] + \frac{q_{bottom}[j]z}{kA} \tag{10}$$

where q is the amount of energy removed from both top and bottom of the cooling blocks, k is the thermal conductivity of the stainless steel, A is the available area for heat transfer, z is the distance between the fluid and thermocouple, and T_{top} and T_{bottom} are the temperature of the top or bottom of the wall respectfully.

Once the local inner wall temperature was determined, the local heat transfer coefficient was calculated. The calculation was as follows:

$$h[j] = \frac{q_{top}[j] + q_{bottom}[j]}{A(T_b[j] - T_w[j])} \quad (11)$$

In this case, A is the area of the all nine parallel channels in a subsection whose length is 50 mm.

Kruizenga *et al.* was able to conclude several items. First, they showed that the heat transfer coefficient decreases as the bulk temperature increases. Also, that as the heat flux in increased, the heat transfer coefficient decreases. Next, one of the significant results Kruizenga *et al.* found was that as the system pressure was increased above the critical pressure, the heat transfer coefficient decreased significantly. Finally, Kruizenga *et al.* compared the calculated Nusselt number to the experimental Nusselt numbers using various known correlations. Kruizenga *et al*. found that the Jackson [20] and Gnielinski [13] correlations typically over predicted the heat transfer while the Dittus Boelter and Pitla correlations performed well across the temperature ranges. Furthermore, it was noted that the Dittus Boelter correlation typically under predicted the values while the Pitla correlation predicted the heat transfer well at low to medium Nusselt numbers but was a bit scattered at the high Nusselt numbers.

CHAPTER III

TEST FACILITY SETUP

In order to properly understand the behavior of supercritical carbon dioxide an experimental analysis must be conducted. Although a computational analysis was done by Sandeep Pidaparti [23] at Texas A&M University, his code is in the beginning stage and requires some improvements. The experimental analysis will be used to validate his simulations the in the future. This section will analyze the experiments that were conducted for this thesis.

Experimental Setup

The work in this thesis began with the construction of an experimental facility. Figure 10 below shows the schematic of the heat exchanger facility that was used in this research.

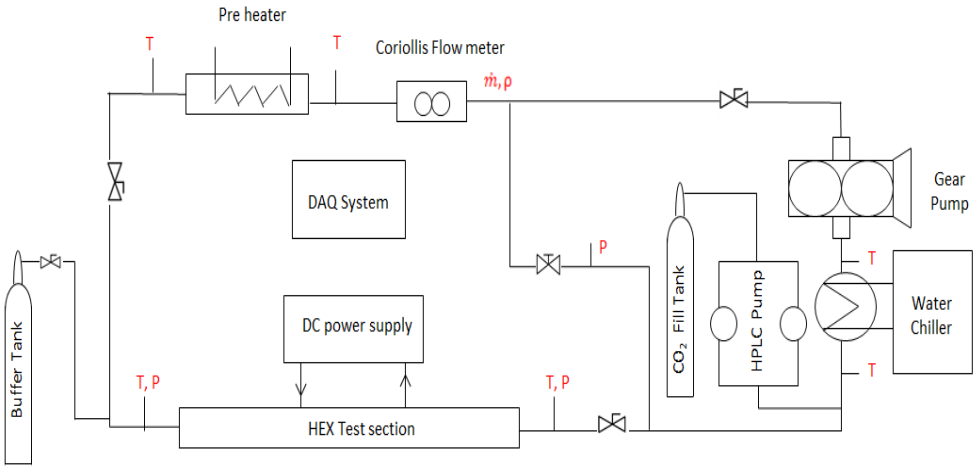

Figure 10: Heat Exchanger Experimental Facility

Carbon dioxide from a cylinder was fed into a Chrom Tech high performance liquid chromatography (HPLC) pump which was used to fill the entire system to the desired pressure. The HPLC pump had a maximum flow rate of 24 mL/min. Typically, this pump filled the system in about 30 minutes to one hour. A Micropump magnetic gear pump powered by a 0.5 hp Baldor-Reliance electric motor was used to circulate the fluid throughout the test loop. The gear pump could supply flow rates as high as 0.05kg/s at about room temperature. However, at elevated temperatures 0.03kg/s was the maximum the pump was able to flow without malfunctions occurring. A Micro Motion Coriolis flow meter was used to measure the mass flow rate of the system. This flow meter was chosen due to its precision of the flow rate measurements. The flow meter could also readily display other important parameters such as density, velocity and volumetric flow rate. A 5.5 kW Tempco preheater was used in the system to raise the temperature of the fluid to the desired test section inlet temperature. This heater was

cartridge type heat. The preheater was custom fitted with connections that allowed it to be readily integrated into our system along with having provisions for thermocouples. A 5kW Magna-Power Electronics DC power supply was used to supply current through the electrically isolated test section to provide the required heat flux. It was calculated that a very large amount of current compared to voltage would be needed to resistively heat the test section. As a result, this power supply was chosen since it can provide 10 V at 500 A. A 5.2 kW Advantage Engineering water chiller unit was used to cool the carbon dioxide down to at least a minimum of room temperature to increase its density for safe use through the gear pump. The chiller unit was used to pump chilled water to a six foot tube-in-tube coiled heat exchanger through which the heated carbon dioxide would pass through in order to cool. Finally, a buffer tank was installed before the test section assembly to reduce the pressure fluctuation caused by the thermostat controlled chiller unit turning on and off. This buffer tank was essentially another carbon dioxide supply tank with modified connections. A National Instruments data acquisition system was used to interface all of the controls and readouts of each component to the LabVIEW program. All major components had Omega Engineering K-type thermocouples at the inlet and outlet of them. Specifications on each of the components can be found in the Appendix. Figure 11 below shows the test facility.

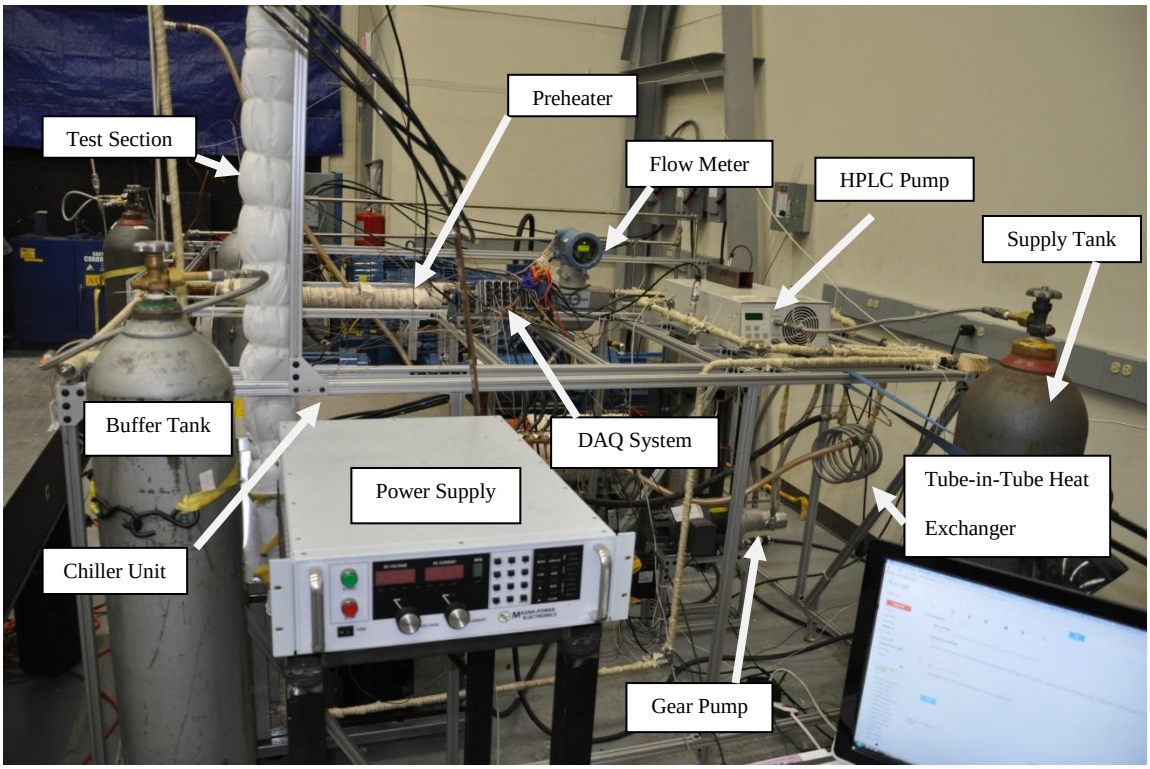

Figure 11: Supercritical Carbon Dioxide Heat Exchanger Facility

Test Section

The test section was simply a straight tube of approximately 1 m. long with an outside diameter (OD) of 0.5 in. and a wall thickness of 0.035 in. The test section was chosen to have a large inner diameter of 0.43 in. It was found that a lot of previous researcher had focused on much smaller diameter tubing. Figure 12 below shows a picture of the test section.

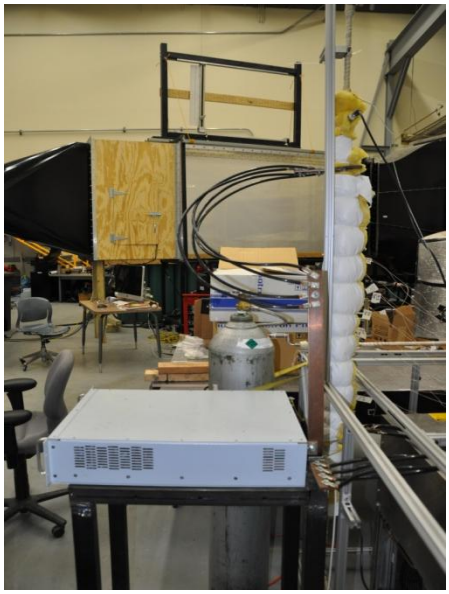

Figure 12: Test Section Used in Experimental Facility

The material of the test section, as well as most other tubing used in the construction of the test facility, was 316 stainless steel. Self adhesive E-type thermocouples from Omega Engineering were attached along the top and bottom surfaces of the heat exchanger at about 3 in. intervals. There were Omega Engineering pressure transducers and resistance temperature detectors (RTD) probed into the flow at the inlet and outlet of the test section.

The first method used to supply the required heat flux was a 627 W tape heater from Omega Engineering that was wrapped around the surface of the test section. This method caused extreme localized heat spots on the test section. Another method was required to provide an even heat flux. The previously mentioned electric power supply was used to provide the required heat flux through resistive heating. Due to the high current requirements, three gauge wire and 0.25 in thick copper bar stock was used to

make the connections between the test section and the power supply. Since the maximum capacity of 3 gauge wire is about 75 amps, four wires had to be used in parallel. Larger gauge of wire could have been used as the expense of difficulty working with the wire due to it being stiffer and harder to manipulate. As shown in Figure 12, copper bar stock was fabricated in such a way that the copper bar stock enclosed the heat exchanger on both sides of the test section and provided a means for four heavy gauge wires to be connected in parallel to one side of the test section.

Thermocouple Calibration

After the test facility was constructed, the thermocouples on the surface of the test section needed to be calibrated. The surface thermocouples were calibrated against the test section inlet RTD under isothermal conditions for temperature ranges from 20-50°C. In other words, the test section inlet would first be set to 20°C. Then, sufficient time was given to allow the surface thermocouples and the inlet RTD that was probed into the flow to reach equilibrium. Afterwards, data was recorded for 500 seconds at a rate of one sample per second. After the data was recorded, averages of each thermocouple's readings were taken. This process was repeated for the temperature range of 20-55°C at 5°C intervals. The averages of each thermocouple reading from 20-55°C were plotted against the inlet RTD temperature. Then a linear curve fit was applied to each thermocouple's data. Finally, the equation of the curve was input into the LabVIEW program for each thermocouple to complete the calibration process.

CHAPTER IV

DATA REDUCTION AND TEST FACILITY VALIDATION

All of the data for this thesis was reduced in the following manner. First, the amount of heat added and removed was calculated using an energy balance across each component assuming steady state and steady flow conditions:

$$\dot{Q}_{CO_2} = \dot{m}(h_{in} - h_{out}) \tag{12}$$

Each component had thermocouples on both the inlet and outlet and the pressure in the entire system was nearly constant. This allowed the enthalpies to be readily calculated. This method differs from the one used by Kim et al. For the total heat into their system, they used strictly the power from the power supply. Their method assumed that nearly all of the thermal energy generated by the power supply would be taken into the system. The method in this thesis used an energy balance on the test section input based on the temperature readings of the bulk of the fluid at the inlet and outlet of the test section from the RTDs probed into the flow.

Second, the inner wall temperatures of the test sections were calculated using a one dimensional steady state conduction heat transfer with heat generation in the test section. The following equation was used to calculate the inner wall temperatures:

$$T_{w,inner} = T_{w,outer} + \frac{\dot{q}}{4k_w}\left[\left(\frac{D_{out}}{2}\right)^2 - \left(\frac{D_{in}}{2}\right)^2\right] - \frac{\dot{q}}{2k_w}\left(\frac{D_{out}}{2}\right)^2 ln\left(\frac{D_{out}}{D_{in}}\right) \quad (13)$$

where $\dot{q}$ is the volumetric flow rate defined as follows:

$$\dot{q} = \frac{Q_{CO_2}}{L(D_{out}^2 - D_{in}^2)\frac{\pi}{4}} = \frac{m(h_{out} - h_{in})}{L(D_{out}^2 - D_{in}^2)\frac{\pi}{4}} \quad (14)$$

Next, the bulk temperature was calculated using a constant heat flux approximation and an energy balance on a differential control volume:

$$T_{b+1} = T_b + \frac{q^{"}\pi Dx}{\dot{m}c_p} \quad (15)$$

T_b was measured by the inlet RTD that was probed into the flow. This approximation was used since using measuring probes in the flow will cause disruption.

Once the bulk temperature was known, the local heat transfer coefficient was calculated as follows:

$$h = \frac{Q_{CO_2}}{A_c\left(T_{w,inner} - T_b\right)} \quad (16)$$

Lastly, once the local heat transfer coefficient was known, the local Nusselt number was calculated with the following equation:

$$Nu_b = \frac{hD_h}{k_b} \tag{17}$$

The experimental Nusselt number was compared to the well know Jackson and Hall Nusselt number. The Jackson Nusselt number was defined by:

$$Nu_{Jackson} = 0.0183 Re_b^{0.82} Pr_b^{0.82} \left(\frac{\rho_w}{\rho_b}\right)^{0.3} \left(\frac{\overline{C_p}}{C_{p,b}}\right)^n \tag{18}$$

The value of n was determined by the bulk temperature using the following criteria [24]:

$$n = 0.4 \; if \; T_b < T_w \leq T_{pc} \; and \; 1.2T_{pc} \leq T_b < T_w$$

$$n = 0.4 + 0.2\left(\frac{T_w}{T_{pc}} - 1\right) \; if \; T_b \leq T_{pc} < T_w$$

$$n = 0.4 + 0.2\left(\frac{T_w}{T_{pc}} - 1\right)\left(1 - 5\left(\frac{T_b}{T_{pc}} - 1\right)\right) \; if \; T_{pc} \leq T_b \leq 1.2T_{pc} \; and \; T_b < T_w$$

Jackson and Hall's correlation can be used to analyze the data for possible effects of buoyancy. In this experiment, the experimental Nusselt number will be normalized with Jackson and Hall's Nusselt number. Typically, for downward flow, if the normalized

Nusselt number is greater than one for bulk temperatures less than the pseudocritical temperatures except the cases where bulk temperature is only slightly less than the pseudocritical temperature, the heat transfer will be enhanced. On the other hand, typically for the upward flow cases, where the normalized Nusselt number is less than one for all of the bulk temperatures less than the pseudocritical temperatures, the heat transfer is deteriorated.

Test Facility Validation

Before the test facility was used with carbon dioxide, the facility was validated using distilled water. Water was chosen as working fluid because there are well published correlations for water. In other words, the water typically behaves in a predictable manner. For the water validation cases, a constant heat flux of 13.5 kW/m^2 was used with an inlet fluid temperature of 25°C, standard room pressure and several mass flow rates. The recorded wall temperatures were then compared to the results obtained using an energy balance with the Dittus Boelter correlation. The Dittus Boelter correlation is as follows:

$$Nu_{DB} = 0.023 Re_b^{0.8} Pr_b^{0.4} \quad (19)$$

After the Nusselt number was calculated, an energy balance was conducted to calculate the theoretical wall temperature. The bulk temperature was calculated using a one-dimensional heat transfer analysis. The wall temperature was calculated as follows:

$$T_{wall} = T_{bulk} + \frac{q^{"} d}{k_b Nu_{DB}} \tag{20}$$

The measured wall temperatures along the test section from surface thermocouples were recorded using a LabVIEW program. Afterwards, the corresponding Nusselt numbers as a function of position along the heat exchanger were recorded. Figure 13 below shows the measured wall temperatures and calculated Nusselt numbers for a system mass flow rate of 0.035 kg/s. For this case, however, the thermocouple spacing was about 3.9 inches. This was due to the system specifications not fully developed at that time. Also, thermocouples were placed from position x=0 m to x=1 m. However, in the figure above, data is not shown for the first three thermocouples. This is due to allowing some distance to let the flow to fully develop. Figure 13 also shows that the experimental values and the theoretical values match within the expected error range.

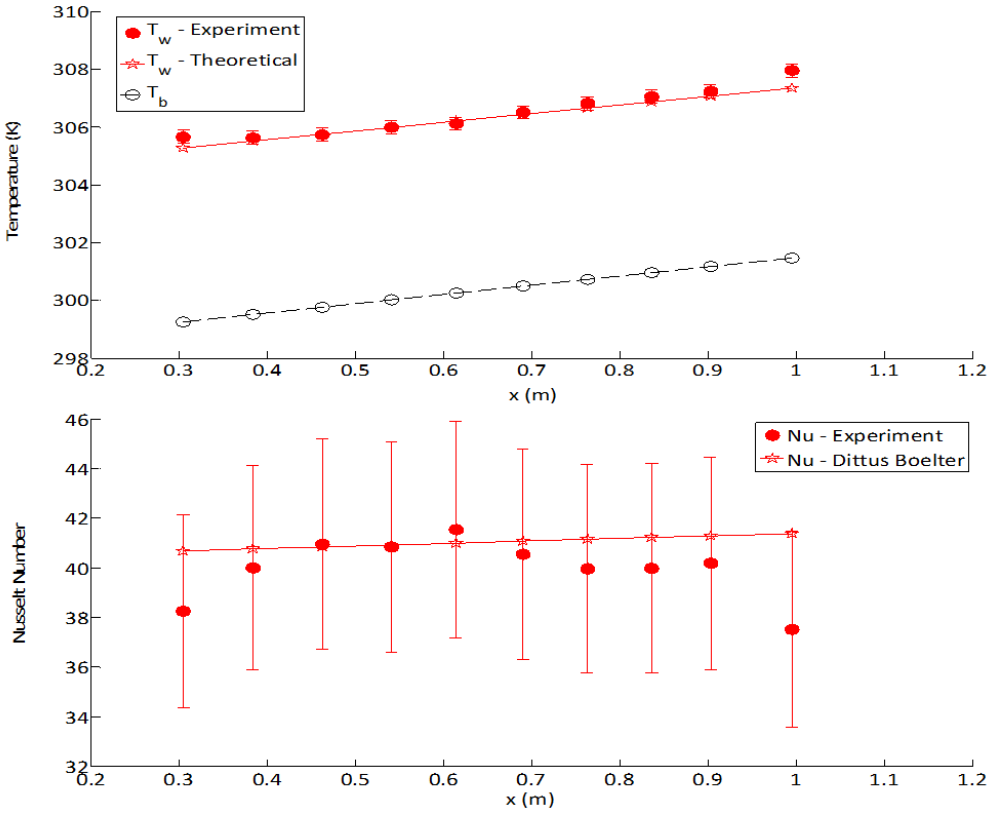

Figure 13: Nusselt Number and Wall Temperature for Distilled Water Validation Case

CHAPTER V

EXPERIMENTAL RESULTS

Experiments were conducted with two mass flow rates, two heat inputs and three pressures. Table 4 shows a test matrix with each of the experimental runs using the different pressures, mass flow rates and heat inputs for both orientations: vertically upward and downward.

Table 4: Test Matrix

Pressure	Mass Flow Rate	Heat Input
7.5 MPa	0.0183 kg/s	540 W
7.5 MPa	0.03 kg/s	955 W
7.5 MPa	0.0183 kg/s	955 W
8.1 MPa	0.0183 kg/s	540 W
8.1 MPa	0.03 kg/s	955 W
8.1 MPa	0.0183 kg/s	955 W
10.2 MPa	0.0183 kg/s	540 W
10.2 MPa	0.03 kg/s	955 W
10.2 MPa	0.0183 kg/s	955 W

The pressure of 7.5 MPa was chosen to represent a pressure just above the critical pressure of carbon dioxide. Choosing a lower pressure than 7.5 MPa would have resulted in damage to the gear pump in the system since there is a possibility for the flow to become two-phase flow. Pumps typically are not designed to operate with two-phase flow flowing through them. The pressures of 8.1 MPa and 10.2 MPa were chosen to represent pressures away from the critical pressure to observe the effects of increasing the pressure. The two mass flow rates were chosen such that one would represent a low mass flow rate, 0.0183 kg/s, and the other a high mass flow rate, 0.03 kg/s. The mass flow rate of 0.03 kg/s was the highest mass flow rate that would allow the test facility to remain stable, particularly at high temperatures and low pressures. Similarly, the heat inputs were chosen to represent a low heat input of 540 W and a high heat flux of 955W.

The following sections will show and analyze the experimental results. The results are divided among the three system pressures.

7.5 MPa Case Results and Discussion

The following are the results of the 7.5 MPa system pressure case. Heat transfer coefficient and Jackson and Hall correlation normalized Nusselt numbers were plotted against a normalized temperature. In all of cases, the normalized temperature was the ratio of the bulk temperature to the pseudocritical temperature, which was discussed earlier.

For the first part, results were obtained using a total heat input of 955W and a mass flow rate of 0.0183 kg/s for both orientations. Figure 14 below shows the results of this case.

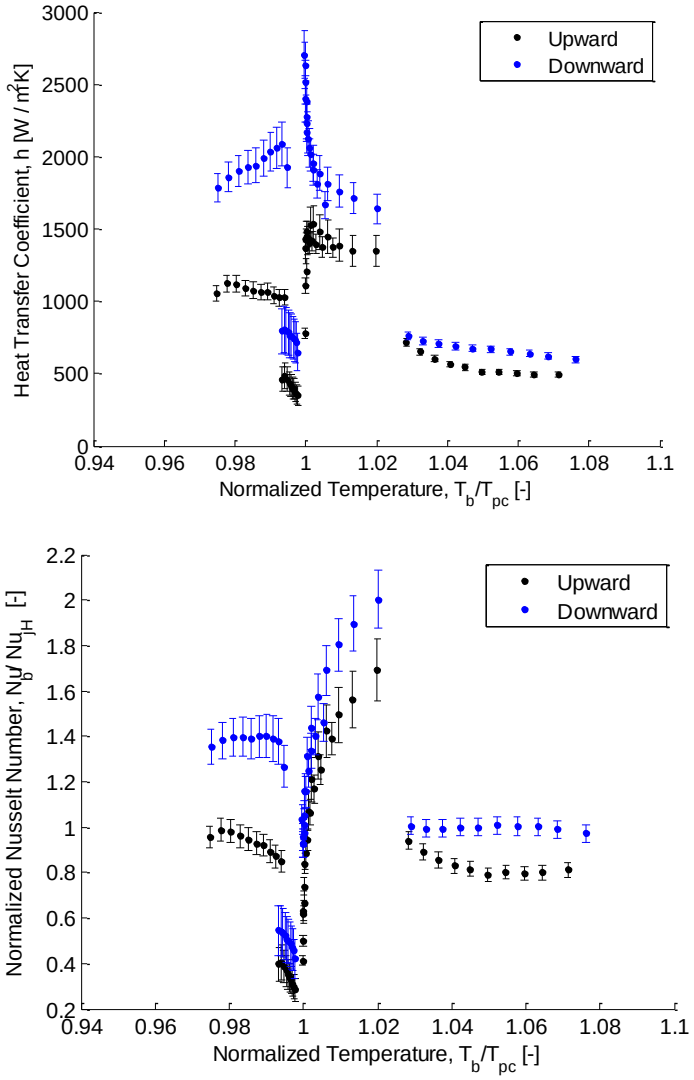

Figure 14: 7.5 MPa Case with 955 W Input and a 0.0183 kg/s Mass Flow Rate Normalized Nusselt Number

As expected, there was a sharp rise in the heat transfer coefficient near the critical point as well as the corresponding Nusselt number. The sharp increase represents the region of heater transfer enhancement. It was observed that the downward flow configuration typically had the higher heat transfer coefficient of the two orientations. Just before the region of heat transfer enhancement, however, heat transfer deterioration was observed as the temperature increased and approached the pseudocritical temperature as shown by the decrease in heat transfer coefficient just before the critical point. This deterioration has been subject to many theories. Typically, these theories involve the effects of buoyancy, acceleration and/or the drastic change in properties associated with supercritical fluids. Kao *et al.* explained this phenomenon as follows. They said that at low flow rates and high heat fluxes, a thin non-conducting layer forms between the interface of the fluid and the inner wall of the heated tubing [25]. This layer prevents heat transfer into the fluid. The non-conducting layer could have been facilitated by the wall temperature being above the pseudocritical temperature and the bulk temperature being lower than the pseudocritical temperature. When this occurs, the properties of the fluid can be drastically altered, in particular, drastic change in density. This density change, in turn can cause buoyancy effects in the flow which enable the aforementioned bubble to form between the fluid and the heated wall surface. This phenomenon is typically believed to be happening at the point on the test section where the wall temperature of a particular point has spiked. For this particular case, the wall temperatures as well as the bulk temperature from three different inlet temperatures are shown in Figure 15 below. At a test section inlet of about 31 °C, there is large spike in

wall temperature for the upward case. This spike corresponds to the point of the large deterioration observed in Figure 14 for the upward orientation. Bulk temperatures are shown to prove that the test section does have a constant wall heat flux. For all subsequent cases, it was found that the wall and bulk temperature grow with approximately the same linear slope for the downward cases, as is typical for constant wall heat flux cases. For the upward cases, the wall temperature spikes prohibited the bulk temperature and the wall temperature to increase with the same slope.

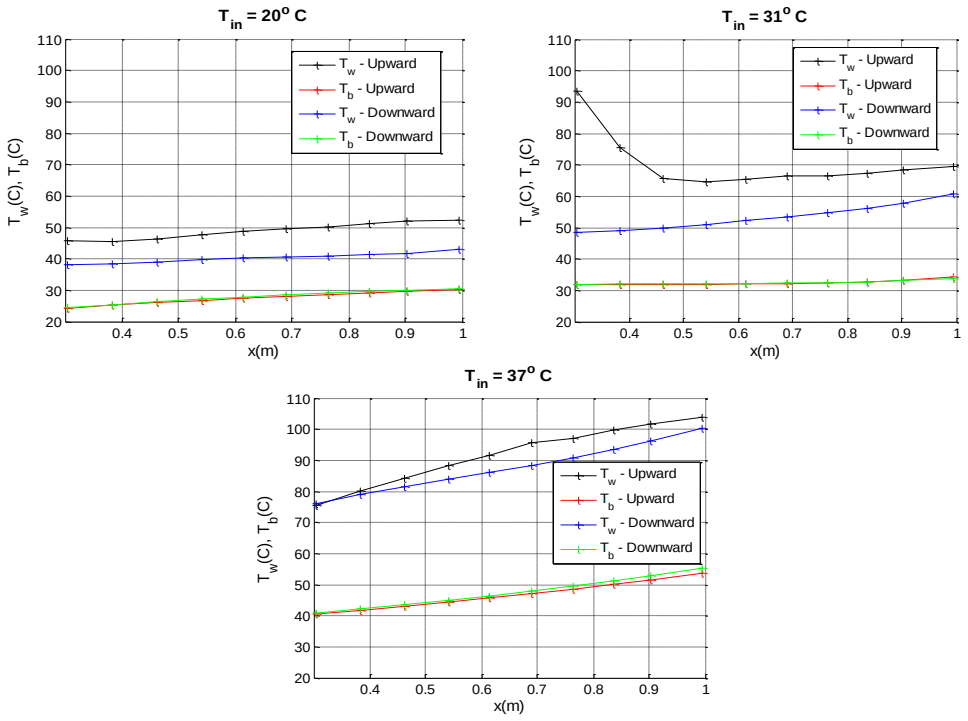

Figure 15: Wall and Bulk Temperatures for 7.5 MPa, 0.0183 kg/s and 955 W Case

A sharp rise in wall temperature was not found for the downward configuration. Also, it is important to notice that since the overall heat transfer coefficients were higher with the downward case, the corresponding wall temperature are lower than the upward case. This signifies that more heat was transfer with the downward orientation compared to the upward orientation. Figure 15 also shows that the overall wall temperature profiles of the upward and downward orientation quite different when the bulk temperature is lower than the pseudocritical temperature. The profiles are quite similar after the pseudocritical temperature. This behavior was observed for all following cases as well. Similar temperature profiles above the pseudo critical temperature also suggest that the temperature profiles are independent of orientation. Finally, Figure 14 shows that the experimental Nusselt number values tend to agree well with the correlation by Jackson and Hall after critical point and are within 50% before the critical point.

The next case involved using the same heat input of 955 W but a higher mass flow rate of 0.03 kg/s. Figure 16 below showed the results of this case.

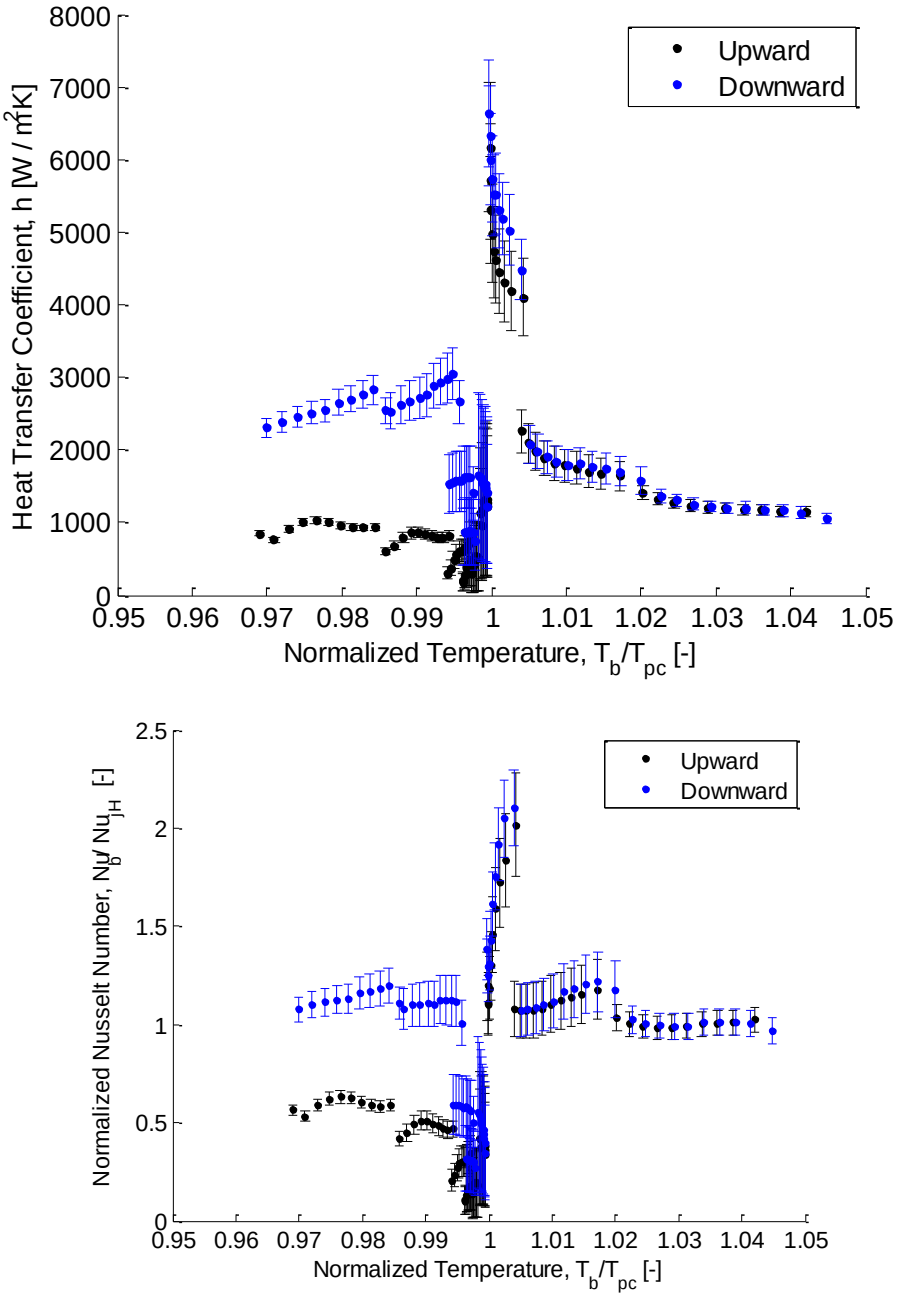

Figure 16: 7.5 MPa Case with 955 W Input and a 0.03 kg/s Mass Flow Rate and Normalized Nusselt Number

In this case, the peak values for the heat transfer coefficient were significantly increased to more than double. This was expected due drastic increase in mass flow rate. Much of the analysis can be compared with the previous case. Again, the wall and bulk temperatures were examined as shown below in Figure 17 below.

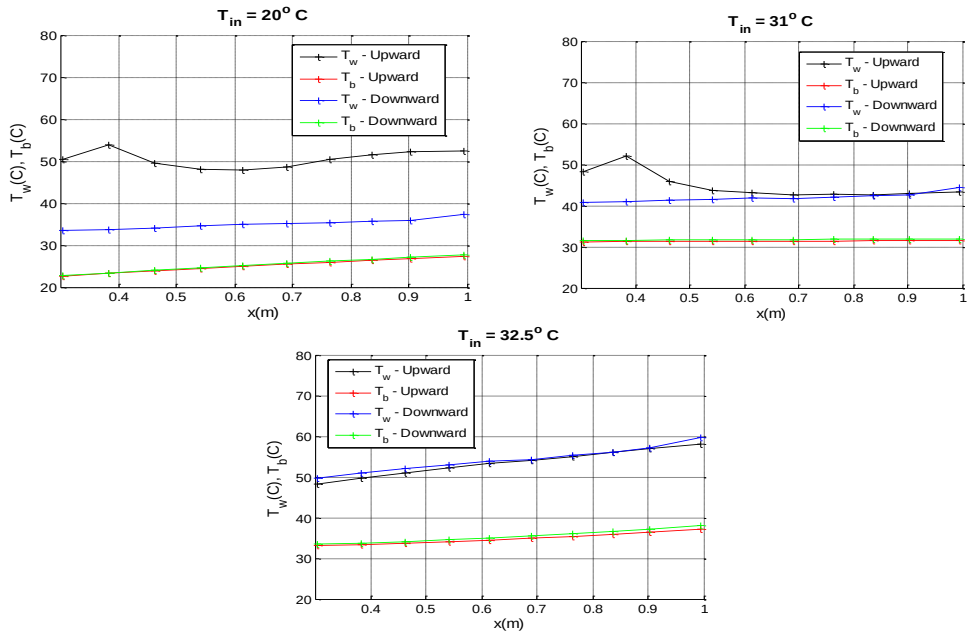

Figure 17: Wall and Bulk Temperatures for 7.5 MPa, 0.03 kg/s and 955 W Case

In this case, a sharp increase in wall temperature was not observed for either orientation. However, there was a region of lower wall temperatures despite an increase in inlet fluid temperature for the upward orientation. This could signify the effects of heat transfer enhancement. Finally, Jackson and Hall's correlation seemed to predict all of the data well after the critical point. Their correlation seemed to predict the downward flow case very well before the critical point and the vertical cases within 50% before the critical point.

In the final 7.5 MPa case, the heat input was lowered to 540W and the mass flow rate was reduced to 0.0183. Figure 18 below shows the results for this case.

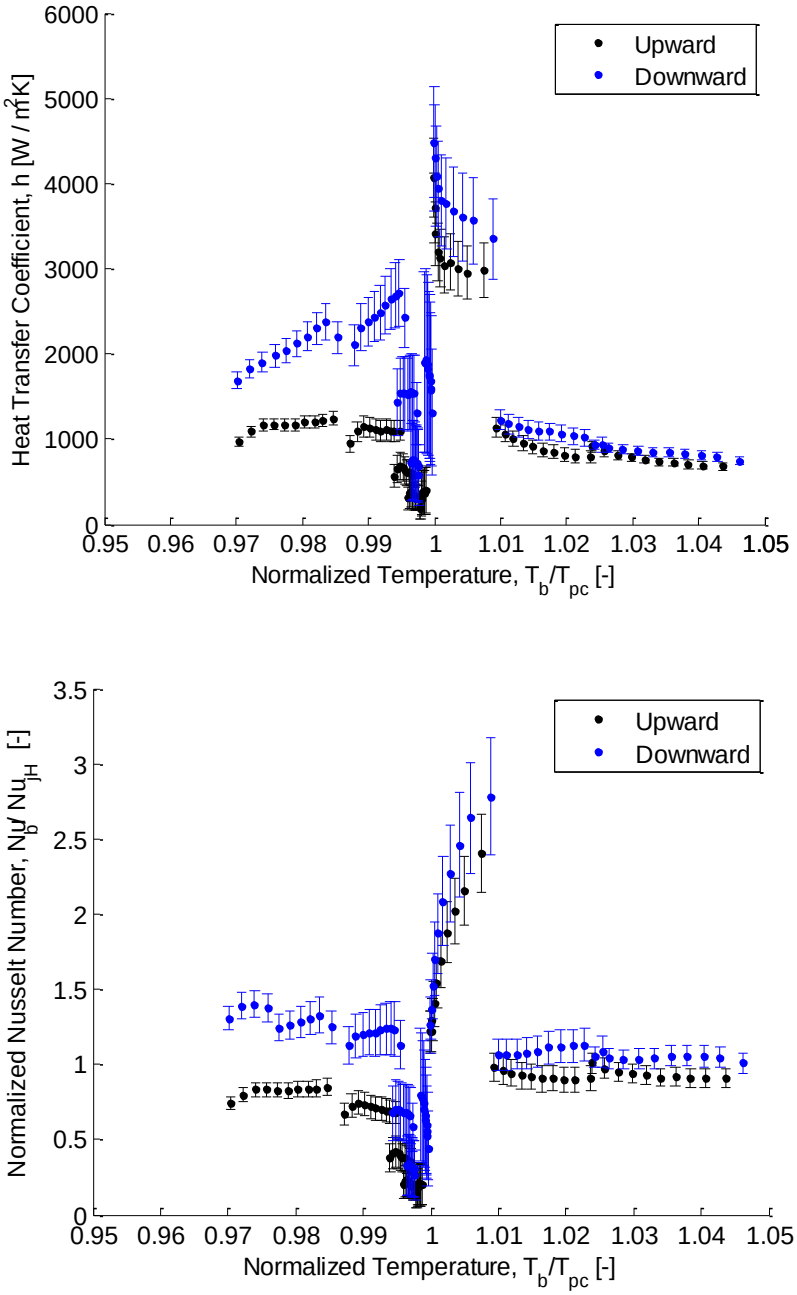

Figure 18: 7.5 MPa Case with 540 W Input and a 0.0183 kg/s Mass Flow Rate and Normalized Nusselt Number

In this case, the peak values for the heat transfer coefficient were significantly high compared to the first case with 955 W of heat input and a mass flow rate of 0.0183 kg/s. This was expected due to having a lower heat flux with the same mass flow rate. This would also help prove what other researchers have said about the correlation of heat flux and deterioration and/or enhancement. The wall and bulk temperatures were analyzed as with the previous two cases. Figure 19 below shows the wall and bulk temperatures for this case.

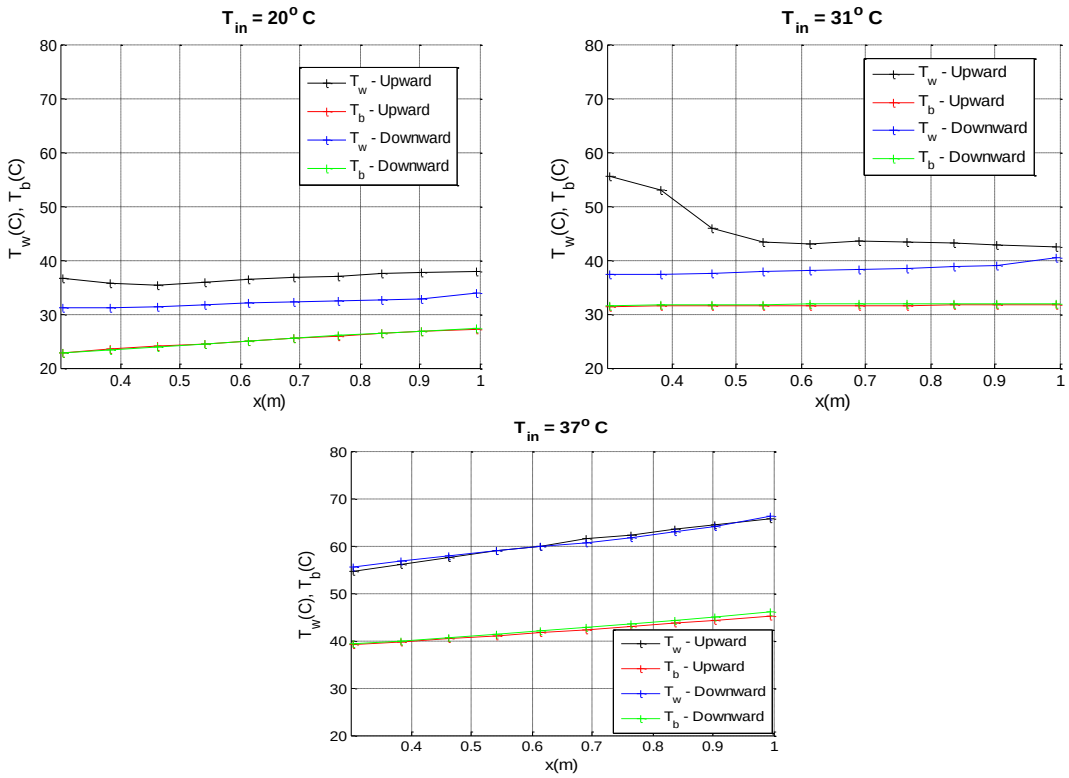

Figure 19: Wall and Bulk Temperatures for 7.5 MPa, 0.0183 kg/s and 540 W Case

In this case, we again see a sharp rise in the wall temperature close to the pseudocritical point for the upward case. The location of this spike corresponds to the point deterioration. Again, Jackson and Hall's correlation seemed to predict all of the data fairly well after the critical point. Similarly, their correlation seemed to predict all of the cases within 50% before the critical point.

It should be noted that higher mass flow rates did seem to allow Jackson and Hall's correlation to predict the behavior of this system better compared to the lower mass flow rates. Also, when the mass flow rate was kept the same, increasing the heat flux seemed to make the results a bit more sporadic. As seen above, when the heat flux was increased, Jackson and Hall's correlation was to not be able to predict the behavior before and after the critical point well.

8.1 MPa Case Results and Discussion

As with the 7.5 MPa case, this case was started with using a heat input of 955 W and a mass flow rate 0.0183 kg/s. Figure 20 below shows the results for this particular case.

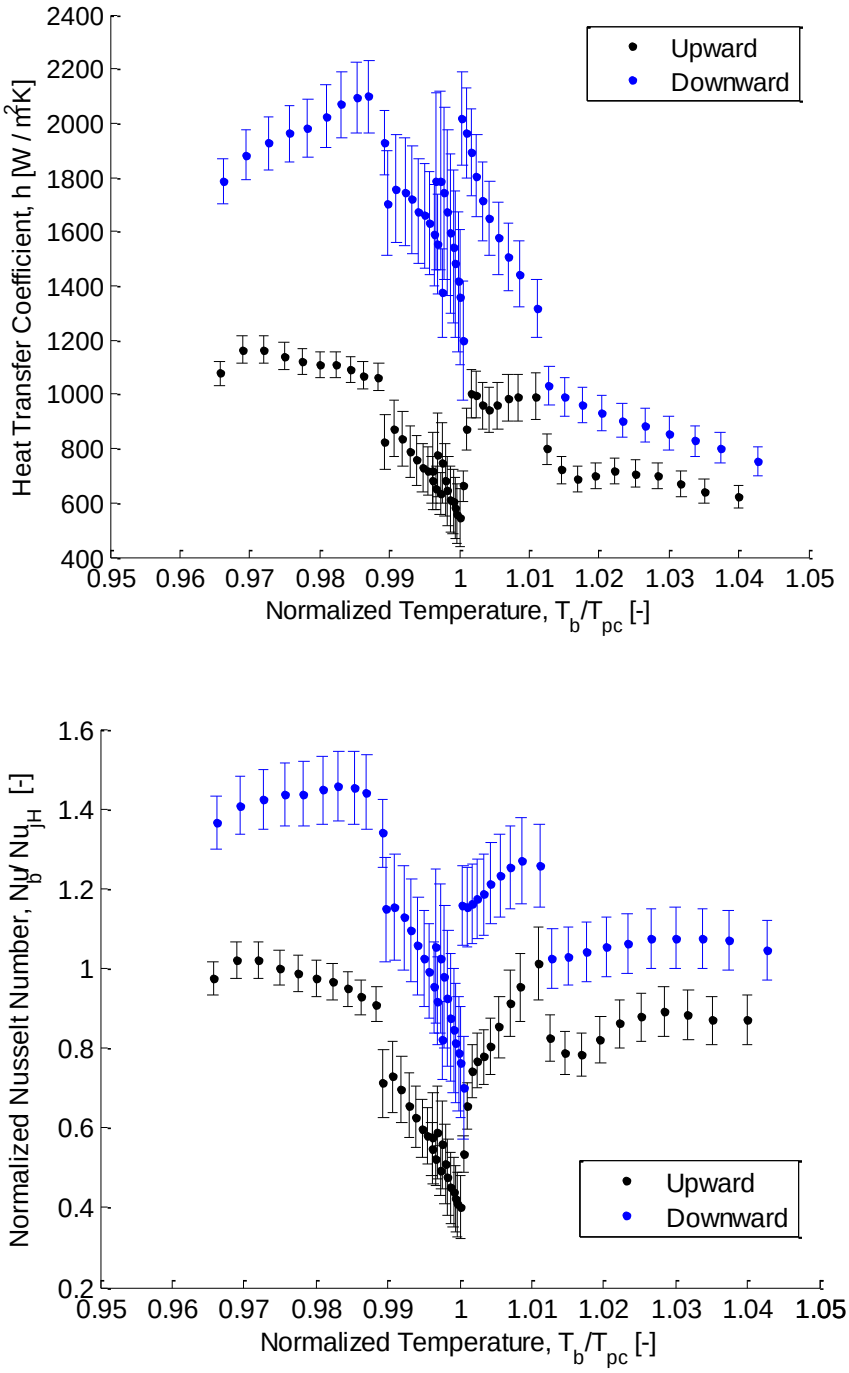

Figure 20: 8.1 MPa Case with 955 W Input and a 0.0183 kg/s Mass Flow Rate and Normalized Nusselt Number

Compared to its 7.5 MPa case counterpart, this 8.1 MPa cases did not seem to have a defined peak at which there was an appreciable heat transfer enhancement. The heat transfer did deteriorate and then increased again. However, after the heat transfer increased, the peak value was still lower that the values before the pseudocritical point. Although, theoretically there should be a peak, it was believed that the peak in this case was simply not captured by the experimental setup. Also, with the higher system pressure, lower amounts of deterioration were observed compared to the 7.5 MPa cases. This agrees with the results of other researchers. The wall and bulk temperatures were once again analyzed as shown below in Figure 21.

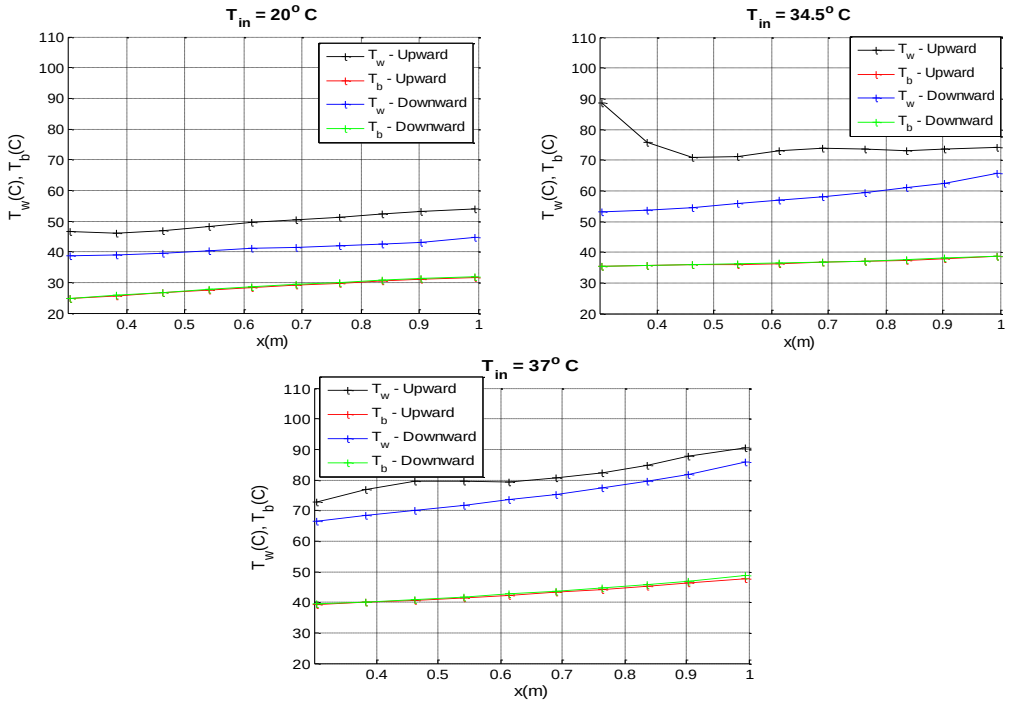

Figure 21: Wall and Bulk Temperatures for 8.1 MPa, 0.0183 kg/s and 955 W Case

For this case, as seen before, there was a sharp increase in wall temperature near the pseudocritical point for the upward orientation. This signified that heat transfer deterioration was present. Additionally, compared to the corresponding 7.5 MPa case, the entire data set was predicted better by Jackson and Hall's correlation. Most of the data was predicted within about 20% before and after the critical point for the upward flow orientation and about within 40% before and after the critical point for the downward flow orientation. Interestingly, Jackson and Hall's correlation seemed to predict the data almost 100% before the pseudocritical point for the upward orientation and after the pseudocritical point for the downward orientation. Also, in this case, less spread in the data was observed at both test section configurations. In other words, Jackson and Hall's correlation seemed to predict this case, particularly the upward orientation very well.

The next case involved using the same heat input of 955 W with a higher mass flow rate of 0.03 kg/s. Figure 22 below shows the results from this case.

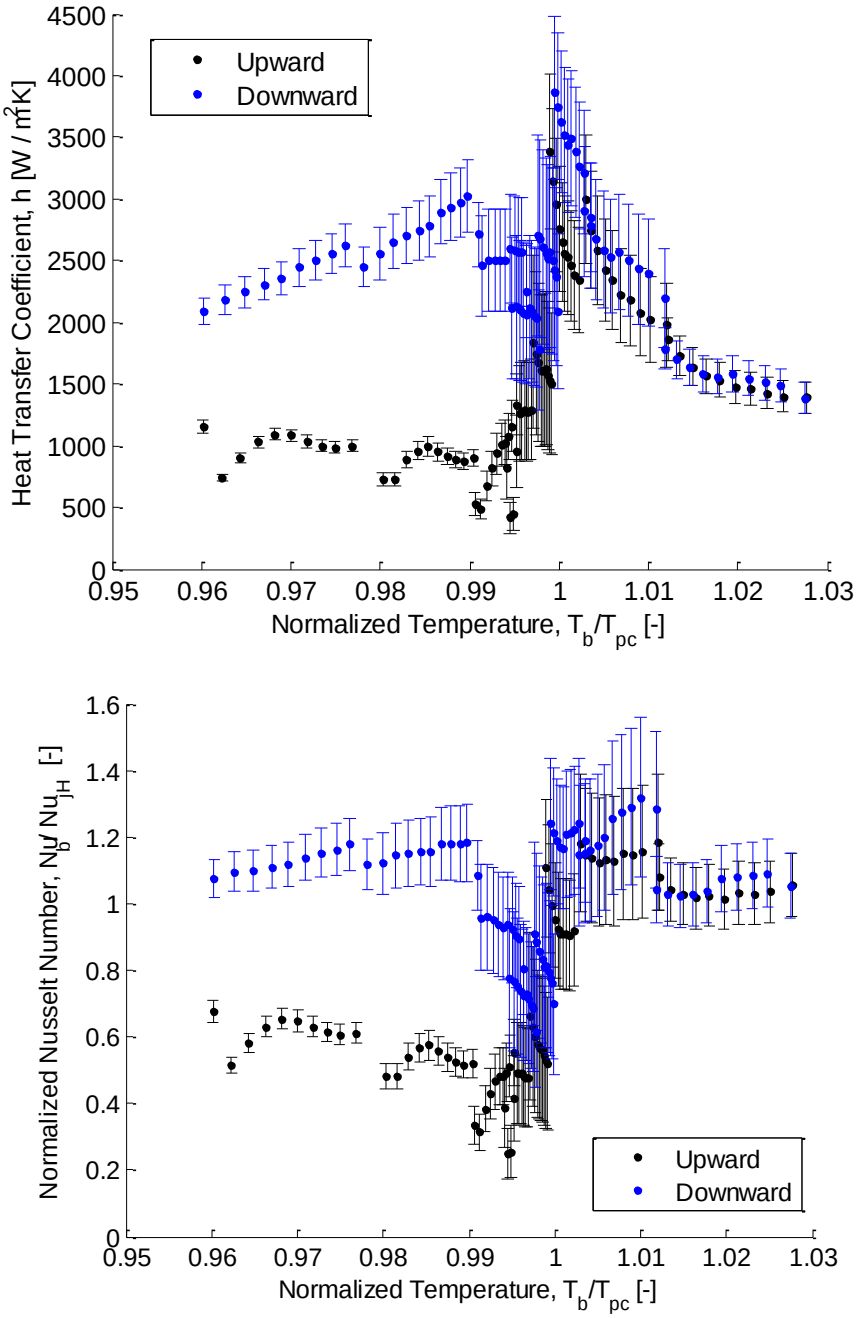

Figure 22: 8.1 MPa Case with 955 W Input and a 0.03 kg/s Mass Flow Rate and Normalized Nusselt Number

Using a higher mass flow rate, peaks in the heat transfer coefficient were once again observed. As pressure increases, a smaller peak value in heat transfer coefficient is expected. This was the case with recorded data in this set as the peak heat transfer coefficient was much lower with a system pressure of 8.1 MPa compared to a system pressure of 7.5 MPa. Figure 23 below shows the wall and bulk temperatures for this case.

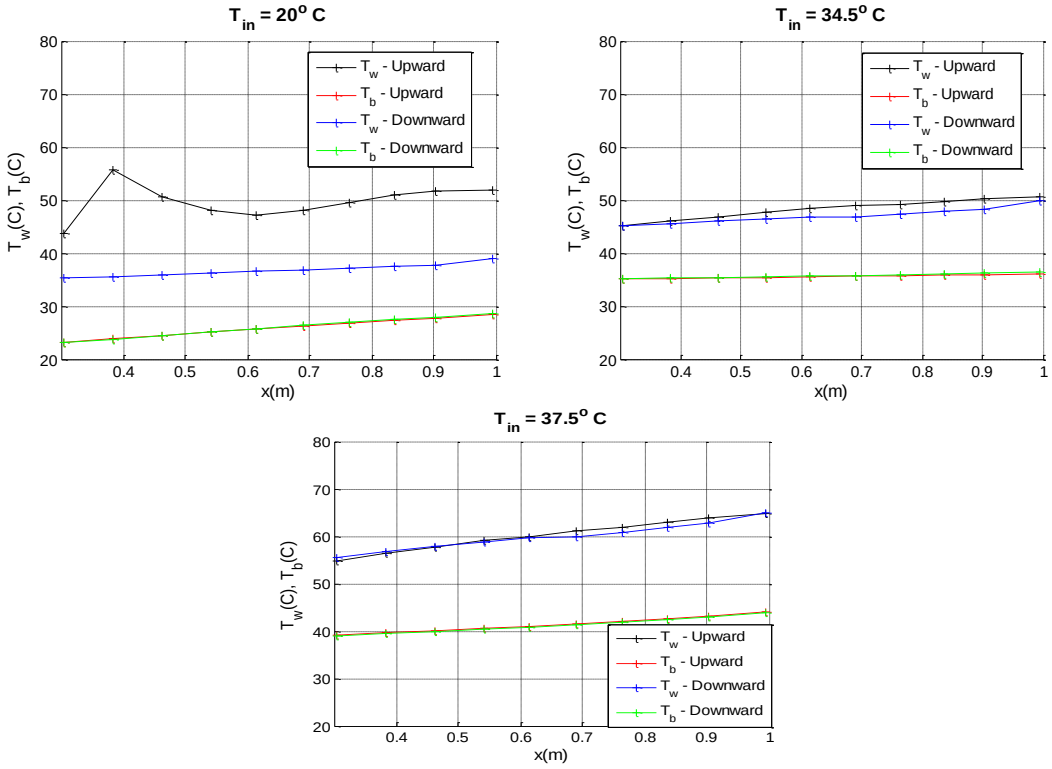

Figure 23: Wall and Bulk Temperatures for 8.1 MPa, 0.03 kg/s and 955 W Case

For this case, no spikes in wall temperature near the pseudocritical point were observed. However, a region of lower wall temperatures was observed after the pseudocritical point. Again, this could indicate a region of heat transfer enhancement. Jackson and

Hall's correlation predicted the data of both orientations very well after the critical point. Their correlation predicted the data well for the downward case before the critical point and the majority of the data within 50% of the upward configurations.

Finally, a combination of the lower heat input of 540 W and the lower mass flow rate were used. Figure 24 below shows the results for this case.

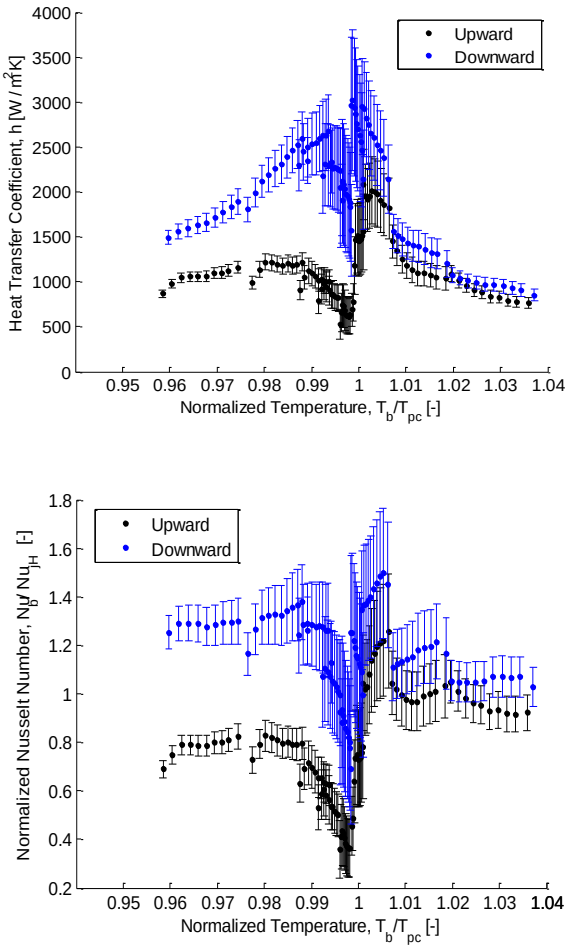

Figure 24: 8.1 MPa Case with 540 W Input and a 0.0183 kg/s Mass Flow Rate and Normalized Nusselt Number

In this, as with the corresponding 7.5 MPa case, the peak value for the heat transfer coefficient were significantly higher compared to the case with 955 W of heat input and a mass flow rate of 0.0183 kg/s. This was, again, due to having lower heat flux with the same mass flow rate. Wall and bulk temperatures for this case are shown below in Figure 25.

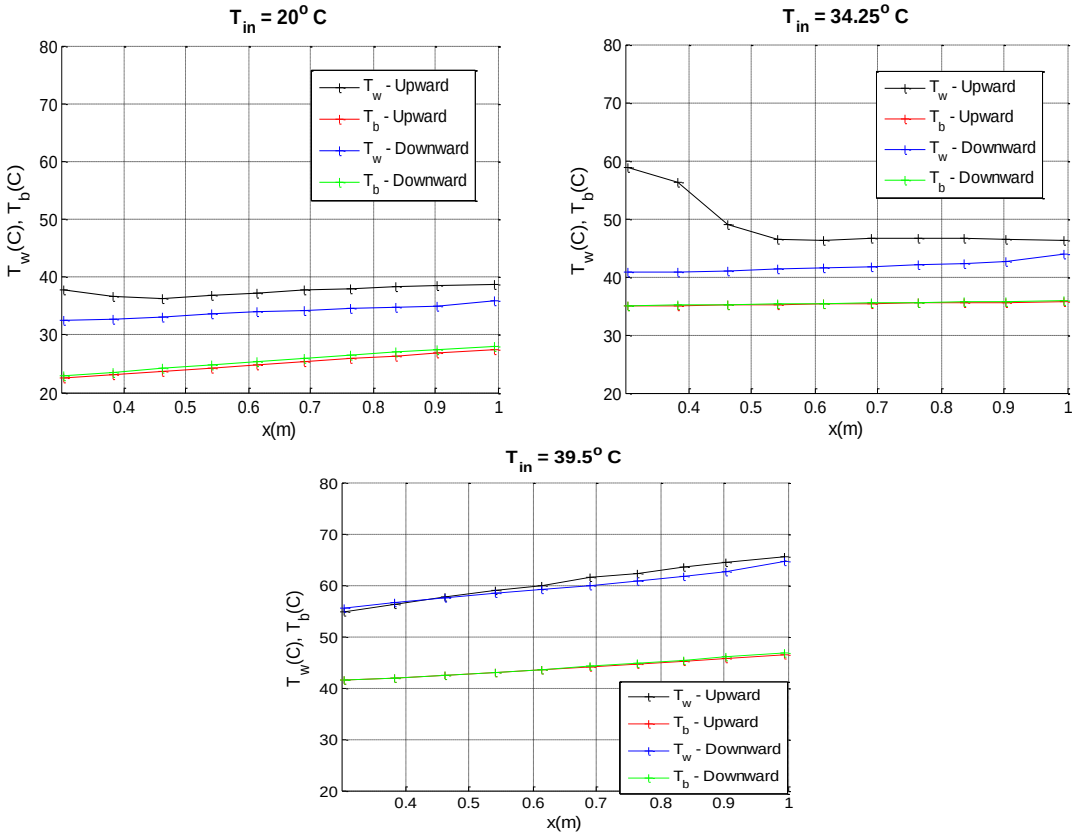

Figure 25: Wall and Bulk Temperatures for 8.1 MPa, 0.0183 kg/s and 540 W Case

There was a spike in wall temperature near the pseudocritical point for the upward case similar to the previous cases. Again, Jackson and Hall's correlation seemed to predict all of the data fairly well, within about 15% after the critical point. Before the critical point,

however, there was significant deviation from Jackson and Hall's correlation. Their correlation predicted the downward configuration within about 40% and the upward configuration within about 70%. The upward configuration seemed to show drastic deviations from Jackson and Hall's correlation before the pseudocritical point. At this time, a definite answer is not available as to why this phenomenon was occurring.

10.2 MPa Case Results and Discussion

The same sequence of results was applied to the final system pressure case of 10.2 MPa. Figure 26 below shows the results for the case using of 955 W of heat input and the lower mass flow rate of 0.0183 kg/s. In this case, there was a no clear sharp rise in the heat transfer coefficient near the pseudocritical point, however, there was still an increase in heat transfer coefficient. Surprisingly, this increase seemed to have occurred before the pseudocritical point. A concrete answer is not available as to why this occurred. It was assumed that thermocouple error may have caused this unusual behavior. As expected with the higher system pressure, the peak value for heat transfer coefficient was significantly lower than the other two pressures.

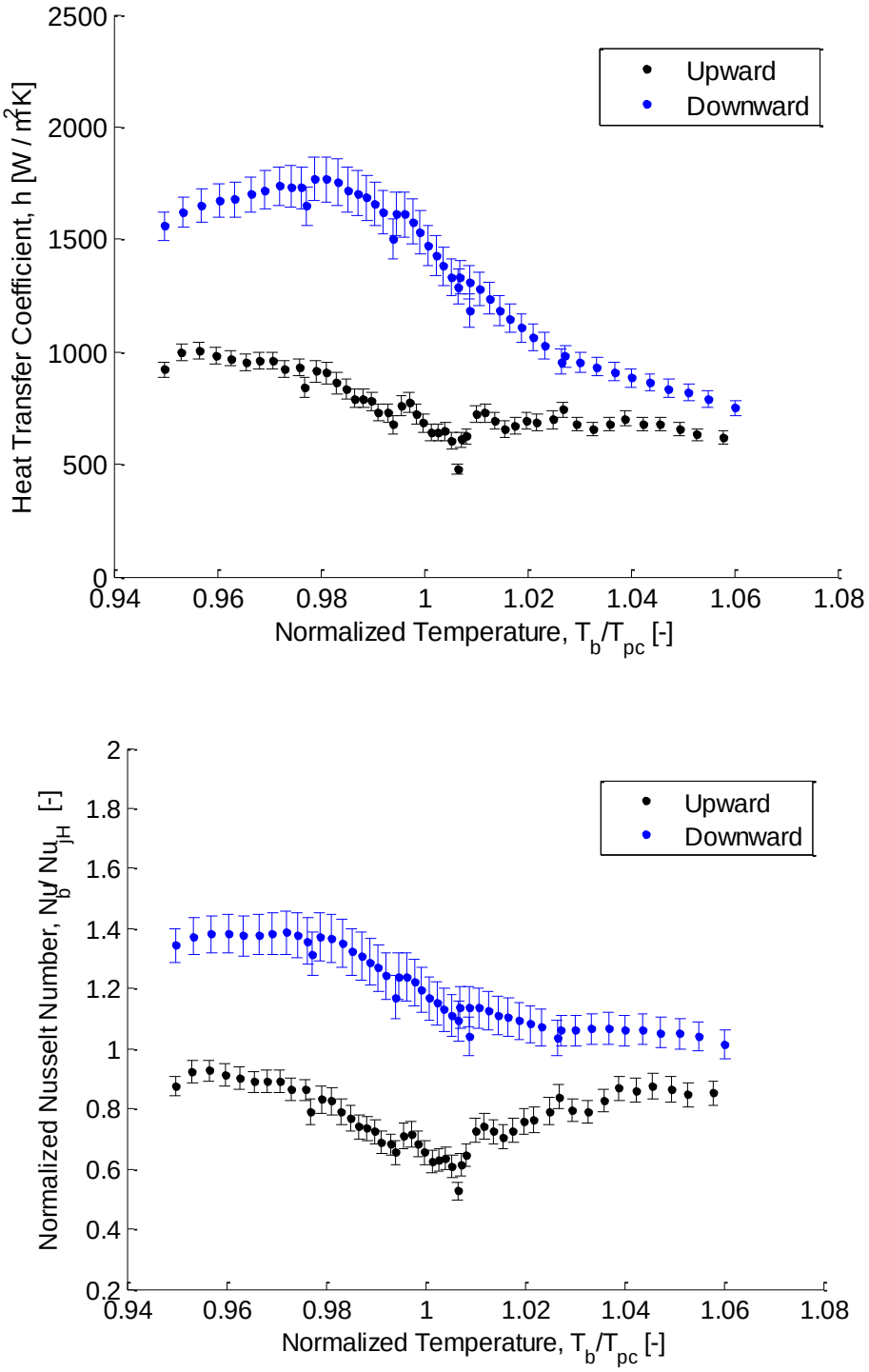

Figure 26: 10.2 MPa Case with 955 W Input and a 0.0183 kg/s Mass Flow Rate and Normalized Nusselt Number

Furthermore, no deterioration was seen in the downward case. However, there was slight deterioration in the upward case near the pseudocritical point. After the point of deterioration for the upward case, the heat transfer coefficient essentially went back to similar values as before the pseudocritical point. Corresponding wall and bulk temperatures are plotted in Figure 27 below.

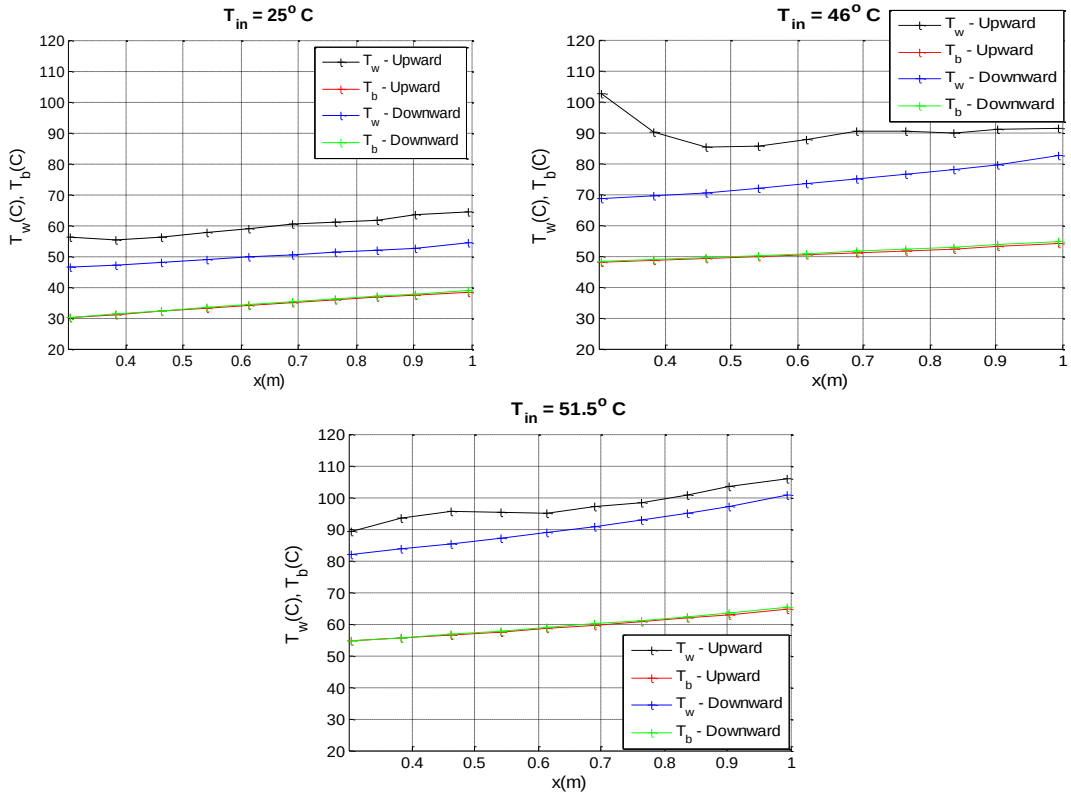

Figure 27: Wall and Bulk Temperatures for 10.2 MPa, 0.0183 kg/s and 955 W Case

A sharp spike in the wall temperature near the pseudocritical temperature point was observed. This is also the same point where the slight deterioration occurred for the upward case. It was observed that the downward flow configuration still had the highest heat transfer coefficient compared to the other two orientations. Jackson and Hall's correlation predicted the data within 40% before the critical point and within about 20% for both orientations.

For the next case, a mass flow rate of 0.03 kg/s and a heat input of 955 W was used. The results from this case are shown below in Figure 28. For this case, the transfer coefficient increased from the previous case as expected. As with the previous case, a sharp peak near the pseudocritical point was not observed for the upward or downward orientations. In fact, in this case, again it appears as though the peak value for the heat transfer coefficient came before the pseudocritical point for the downward case. At this time, a concrete explanation is not available as to why this was occurring. It was assumed that thermocouple error may have played a role in this. In the upward orientation, the peak values in heat transfer coefficient did seem to occur near the pseudocritical point. However, an appreciable heat transfer increase near the pseudocritical point was not observed.

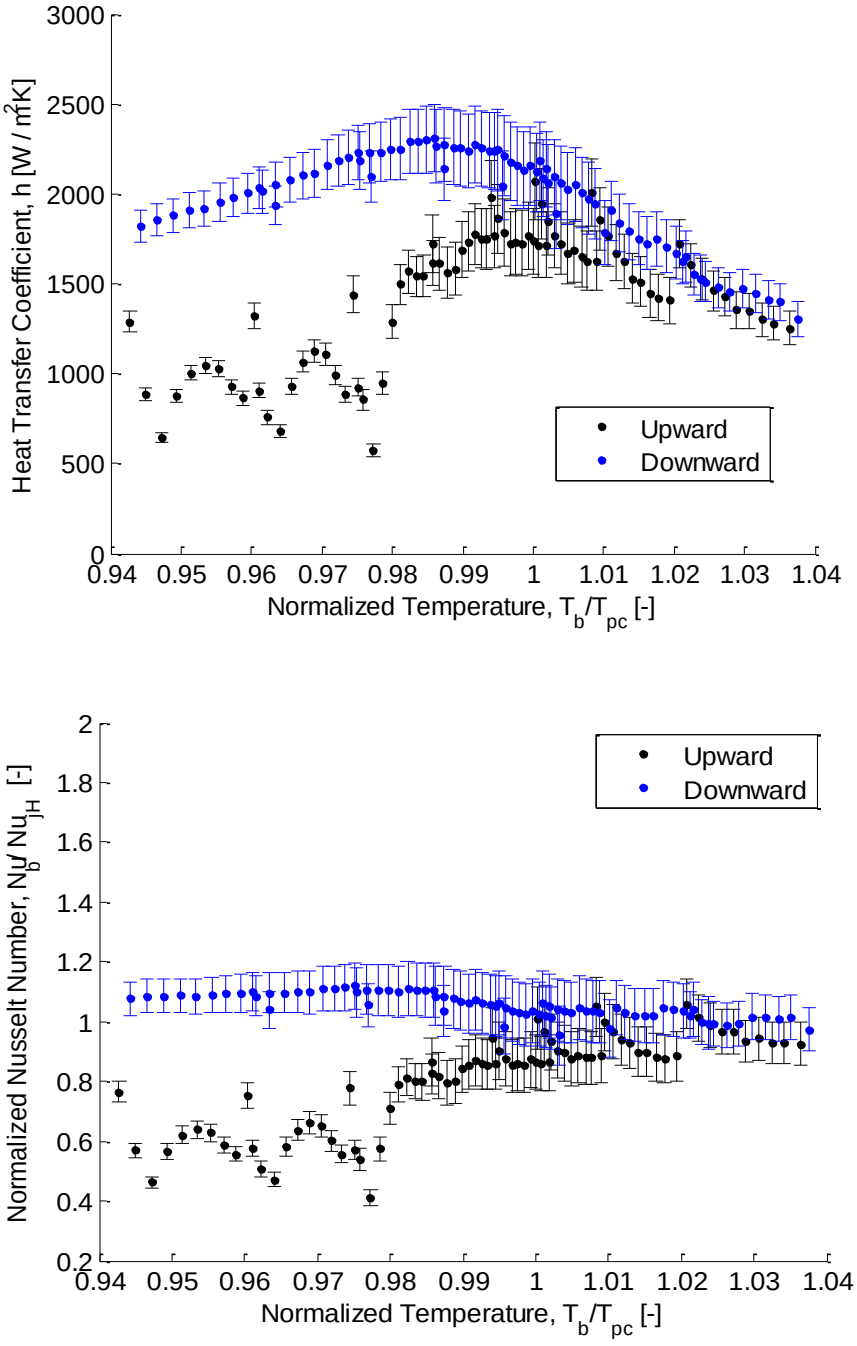

Figure 28: 10.2 MPa Case with 955 W Input and a 0.03 kg/s Mass Flow Rate and Normalized Nusselt Number

For this case, deterioration was not observed in either of the orientations. Corresponding wall and bulk temperatures for this case are plotted in Figure 29 below.

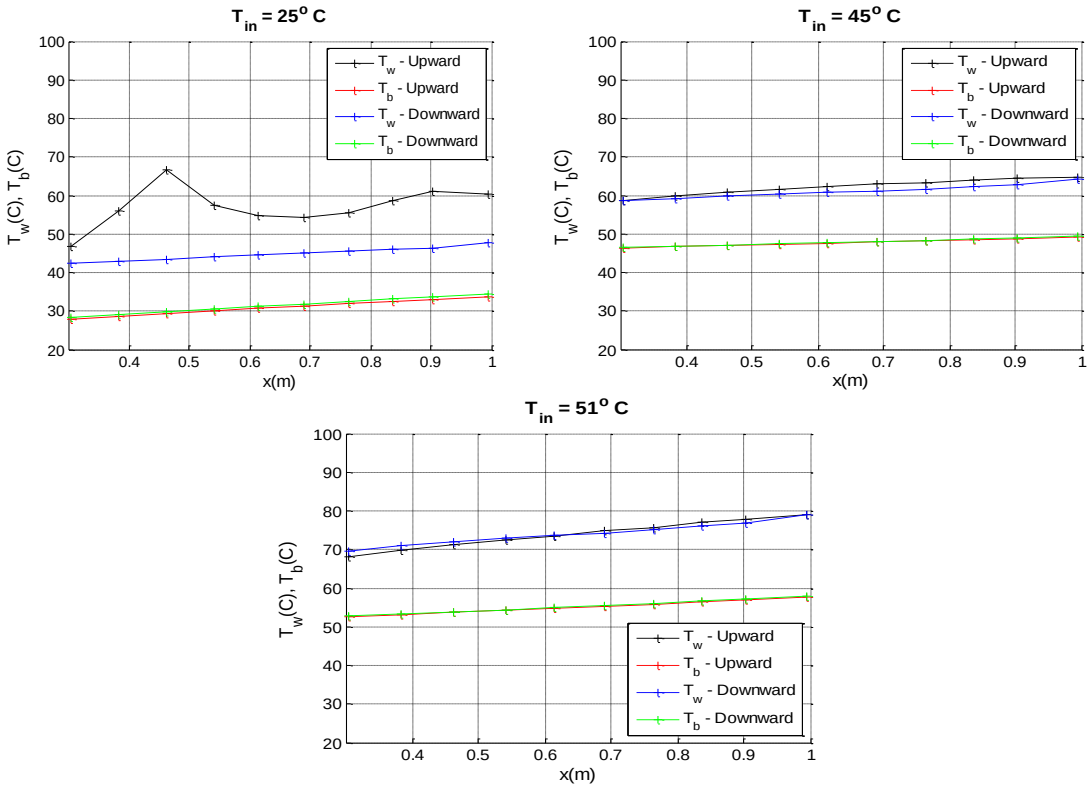

Figure 29: Wall and Bulk Temperatures for 10.2 MPa, 0.03 kg/s and 955 W Case

A sharp spike in the wall temperature much before the pseudocritical temperature point was observed. In this case, however, a significant deterioration was not observed at the location where the spike in wall temperature occurred. It was observed that the downward flow configuration still had the highest heat transfer coefficient compared to the other two orientations. Jackson and Hall's correlation predicted the data within 60% before the pseudocritical point and within about 20% after the pseudocritical point. The

effects of buoyancy for the downward case seem to be significantly less than the upward case before the pseudocritical point.

Finally, the last case with a system pressure of 10.2 MPa had a mass flow rate of 0.0183 kg/s and a heat input of 540 W. Results for this case are shown below in Figure 30. For this case, there was deterioration as well as enhancement for the upward orientation case near the pseudocritical point. In the downward orientation, however, there seemed to be only a small rise in heat transfer coefficient slightly before the pseudocritical point. However, due to the high error, it is difficult to say whether there is heat transfer deterioration and/or enhancement near the pseudocritical point for this orientation by looking only at the heat transfer coefficient. For this reason, the wall temperatures along the test section were analyzed to see if a conclusion could be drawn about the present of deterioration.

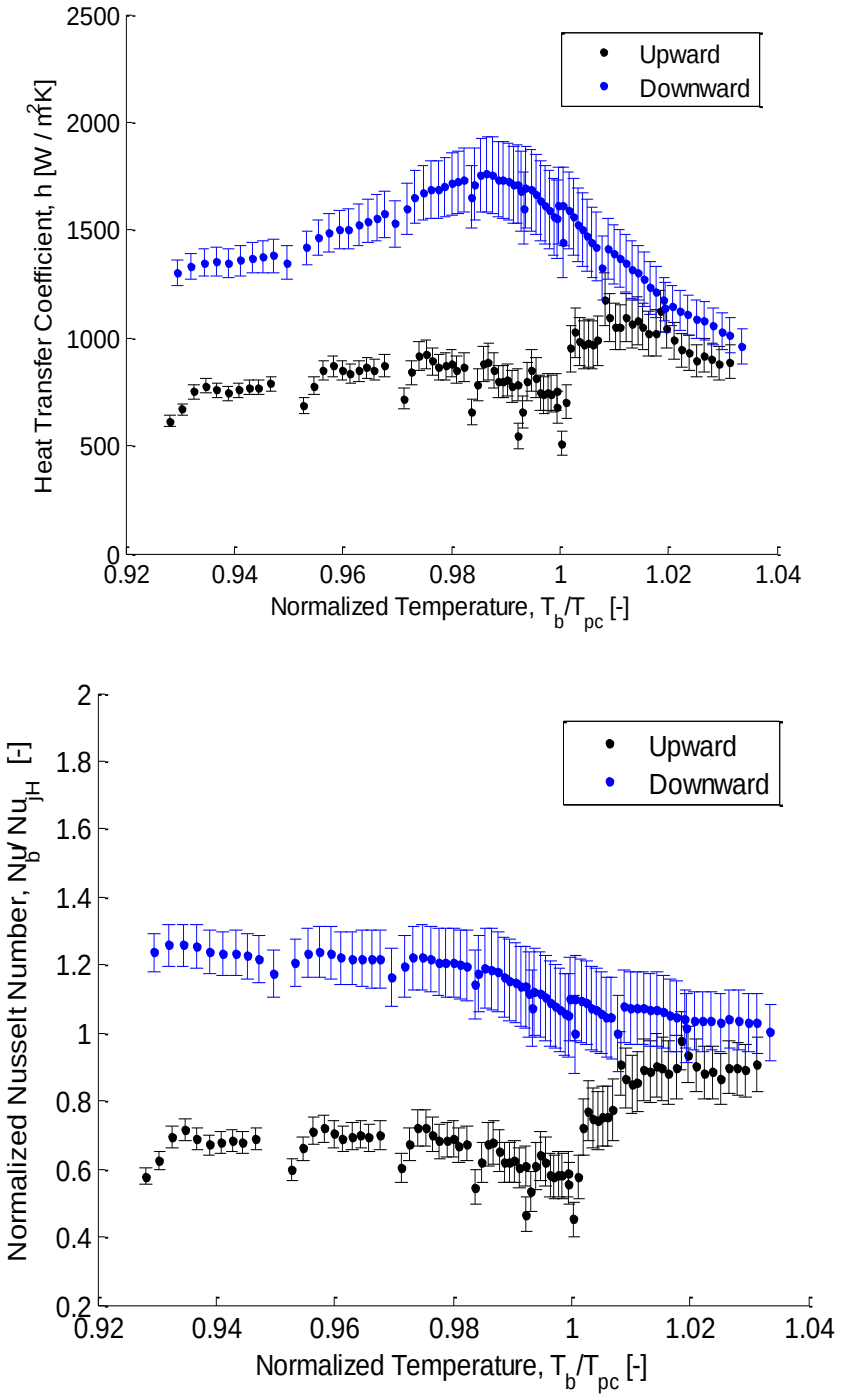

Figure 30: 10.2 MPa Case with 540 W Input and a 0.0183 kg/s Mass Flow Rate and Normalized Nusselt Number

Figure 31 below shows the corresponding wall and bulk temperatures for this case.

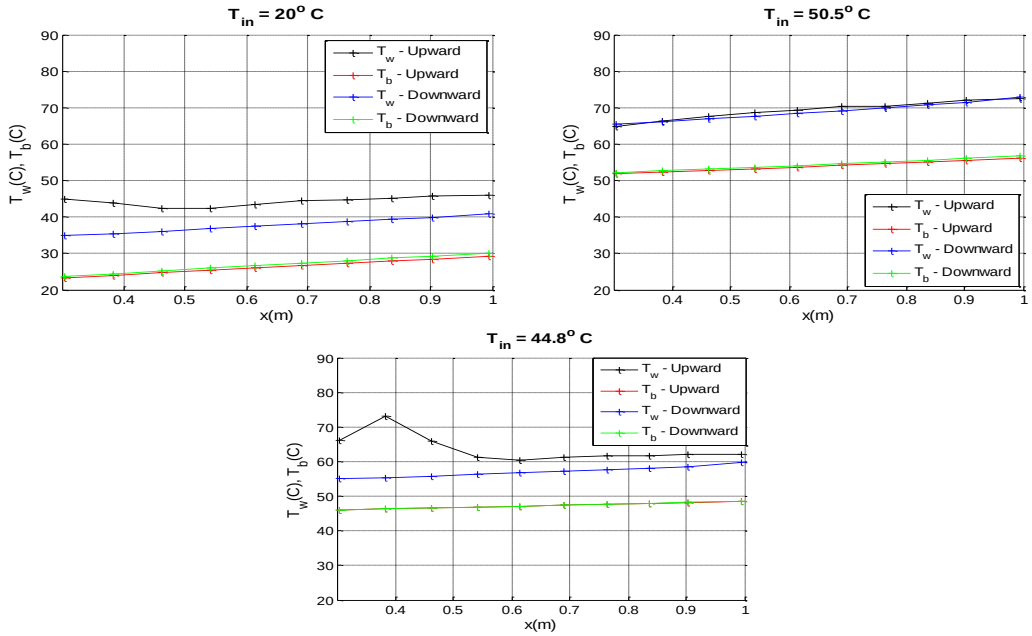

Figure 31: Wall and Bulk Temperatures for 10.2 MPa, 0.0183 kg/s and 540 W Case

Looking at the wall temperatures, there was a spike in wall temperature near the pseudocritical temperature for the upward orientation. This would imply that heat transfer deterioration was present for the upward case. However, solid conclusions about heat transfer deterioration and enhancement cannot be drawn for the downward case due to high uncertainty. Jackson and Hall's correlation was again able to predict the data within 40% before the critical point and within 20% after the critical point.

CHAPTER VI

CONCLUSIONS

As the world continues to progress technologically and the world's population continues to increase, the demand for energy will only increase. Finding new sources of power and harnessing that power efficiently, are becoming two very important things to do to keep up with the ever-growing energy demand. There has been a proposal made to use supercritical carbon dioxide in a Brayton cycle in one of the Generation IV nuclear power plant designs. Supercritical carbon dioxide has received attention due to its ability to allow a Brayton cycle to be easily tuned to operate at lower pressure and temperature compared using supercritical water. The large fluctuation in properties can be utilized to design more compact component such as turbines and heat exchangers.

In order to gain more knowledge about the behavior of supercritical carbon dioxide in heat exchangers, an essential component to nearly all power plants, this study was performed. An experimental test facility was constructed to analyze the behavior of supercritical carbon dioxide in a vertically upward and downward flowing heat exchanger with constant heat flux. Following the experimental analysis, some conclusions can be made. First, the downward flow orientation seemed to provide significantly more heat transfer compared to the upward flow orientation near the pseudocritical point. Away from this point, the heat transfer coefficients of both orientations were similar for nearly all cases. Nearly all of the 7.5 MPa and 8.1 MPa

cases present had a region of heat transfer deterioration before a region of heat transfer coefficient enhancement.

Second, buoyancy seemed to play a significant part on heat transfer performance for both the upward and downward orientations. It was found that typically, buoyancy enhanced heat transfer for the downward flow cases and deteriorated heat transfer in the upward flow cases.

Third, if designing component to be used to supercritical fluid, it is most advantageous to design them to operate at close to the critical or pseudocritical point. At this point, the heat transfer reaches a maximum value. It is very important to remember that if operating at the critical point, the slightest fluctuations in pressure or temperature can force the flow into two-phase flow. Two-phase flow is damaging to most pump and possibly other components.

Finally, with this experimental facility, the findings of previous researchers were observed. Heat transfer deterioration and enhancement were observed in a similar manner to other researchers. This helps provide additional validity to the experimental setup.

CHAPTER VII

FUTURE WORK

Since the experimental facility has been validated for vertical flows, an experimental study with horizontal flows will also be properly conducted. Experiments were conducted with the horizontal orientation. However, at that time, thermocouples where not attached along the entire bottom of the test section. It was later observed that there is a significant difference between temperatures of the top and bottom of the test section. Figure 32 below shows an experimental case that was conducted as well as a simulation provided by Sandeep Pidaparti.

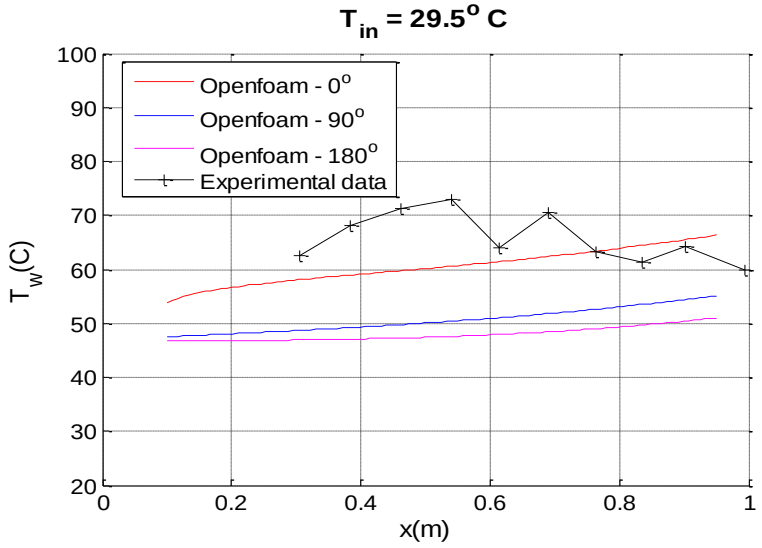

Figure 32: Horizontal Case, Inlet Temperature of 29.5 °C, Wall Temperature Variance in Radial Direction

For this case, the inlet temperature was 29.5 °C. Simulations showed that for this orientation, wall temperature varied heavily with the radial direction. Note that the experimental run wall temperatures are very chaotic. All of the horizontal cases will be reran and analyzed in the same rigorous detail that the previous cases in this thesis were analyzed with.

Second, actual printed circuit heat exchangers can be used in place of the straight tube heat exchanger. Printed circuit heat exchangers of various geometries in addition to the ones described previously can be studied in further detail with this facility. This will allow for better design of heat exchangers for Brayton cycle power plants among other uses for the heat exchangers.

After the computational code has been finalized by Sandeep Pidaparti, his work in conjunction with the experimental results obtained from this research will be used to try and obtain a correlation. This correlation, such as the numerous correlations presented in this thesis, will help to better predict the behavior of not only supercritical carbon dioxide, but hopefully, supercritical substances in general.

Finally, an optical set up will be implemented in this facility. The set up will enable the study of the flow of supercritical carbon dioxide over a heated cylinder. This setup will enable the further understanding of the behavior of supercritical carbon dioxide. The optical set up will also enable the future users to actually see the supercritical state of matter.

REFERENCES

1. *Generation IV Nuclear Reactors*. World Nuclear Association [Report Summary] July 2013 [cited 2014 February 24, 2014]; Available from: http://www.world-nuclear.org/info/Nuclear-Fuel-Cycle/Power-Reactors/Generation-IV-Nuclear-Reactors/.

2. Matsuo, B.K., *A Computational Study of the Thermal-Hydraulic Behavior of Supercritical Carbon Dioxide in Various Printed Circuit Heat Exchanger Designs*, in *Mechanical Engineering*. 2013, Texas A&M University: College Station, Texas. p. 111.

3. Li, Q., et al., *Compact heat exchangers: A review and future applications for a new generation of high temperature solar receivers.* Renewable and Sustainable Energy Reviews, 2011. 15(9): p. 4855-4875.

4. Klein, S.A., *Engineering Equation Solver*. 1992-2013.

5. Liao, S.M. and T.S. Zhao, *Measurements of Heat Transfer Coefficients From Supercritical Carbon Dioxide Flowing in Horizontal Mini/Micro Channels.* Journal of Heat Transfer, 2002. 124: p. 413-420.

6. Dostal, V., P. Hejzlar, and M.J. Driscoll, *The supercritical carbon dioxide power cycle: comparison to other advanced power cycles.* Nuclear technology, 2006. 154(3): p. 283-301.

7. Wischnewski, B., *peace software*. [cited 2013 August 1, 2013]; Available from: http://www.peacesoftware.de/einigewerte/calc_co2.php5.

8. McFarland, J. *Dr. Devesh Ranjan Lab Meeting*. in *Lab Meeting*. 2013. University Servies Building, Texas A&M University, College Station, TX.

9. Steven A. Wright, T.M.C., and Gary E. Rochau, *Overview of Supercritical CO_2 Power Cycle Development at Sandia National Laboratories*. 2011 [cited 2013 August 2, 2013]; Available from: http://www.netl.doe.gov/publications/proceedings/11/utsr/pdf/wed/Wright%20SCO2%20Power%20Cycle%20Summary%20UTSR%202011%20v2a.pdf.

10. Dostal, V., P. Hejzlar, and M. Driscoll, *High-Performance Supercritcal Carbon Dioxide Cycle for Next-Generation Nuclear Reactors.* Nuclear Technology, 2006. 154: p. 265-282.

11. Bazargan, M. and M. Mohseni, *A New Analysis of Convection Heat Transfer Deterioration on Basis of Variations of Eddy Viscosity and Fluid Properties of Supercritical Fluids*. 1999: K.N. Toosi University of Technology, Tehran, Iran.

12. Pitla, S.S., E.A. Groll, and S. Ramadhyani, *New correlation to predict the heat transfer coefficient during in-tube cooling of turbulent supercritical CO_2* International Journal of Refrigeration, 2002. 25: p. 887-895.

13. Gnielinski, V., *New equation for heat and mass transfer in turbulent pipe and channel flow.* International Chemical Engineering, 1975. 16: p. 359-368.

14. Petrov, N.E., and Popvov, V.N., *Heat transfer and resistance of carbon dioxide being cooled in the supercritical region.* Thermal Engineering, 1985. 32(3): p. 131-134.

15. Baskov, V.L., Kuraeva, I.V., and Protopopov, V.S., *Heat transfer with the turbulent flow of a liquid at Supercritical Pressure in tubes under cooling conditions.* Teplofizika Vysokikh Temoperatur, 1997. 15(1): p. 96-102.

16. Krasnoshechekov, E.A., Kuraeva, I.V., and Protopopov, V.S., *Local heat transfer of carbon dioxide at supercritical pressure under cooling conditions.* Teplofizika Vysokikh Temperatur, 1970. 7(5): p. 922-930.

17. Cheng, L., Ribatski, G. and Thome, J.R., *Analysis of supercritical CO_2 cooling in macro- and micro-channels.* International Journal of Refrigeration, 2008: p. 1301-1316.

18. Bae, Y.Y., *Mixed Convection Heat Transfer to Carbon Dioxide Flowing Upward and Downward in a Vertical Tube and an Annular Tube.* Journal of Nuclear Engineering and Design, 2011: p. 305-353.

19. Carlson, M., et al., *Heat Transfer and Pressure Drop of Supercritical Carbon Dioxide Flowing in Several Printed Circuit Heat Exchanger Channel Patterns*, in *International Congress on Advances in Nuclear Power Plants*. 2012: Chicago, USA.

20. Jackson, J.D. and W.B. Hall, *Turbulent forced convection in channels and bundles 2* Forced convection heat transfer to fluids at supercritical pressure. 1979.

21. Kim, H.Y., Kim, H., Song, J.H., Cho, B.H. and Bae, Y.Y., *Heat Transfer Test in a Vertical Tube Using CO_2 at Supercritical Pressure* Journal of Nuclear Science and Technology, 2007. 44: p. 285-293.

22. Kruizenga, A., et al., *Heat Transfer of Supercritical Carbon Dioxide in Printed Circuit Heat Exchanger Geometries* Journal of Thermal Science and Engineering Applications, 2011. 3: p. 1-8.

23. Pidaparti, S., *Heat Exchanger Loop Simulations*, E. Umrigar, Editor. 2012-2014.

24. Kakac, S. and Spalding, D.B., *Turbulent Forced Convection in Channels and Bundles Influences of buoyancy on heat transfer to fluids flowing in vertical tubes under turbulent conditions*. Influences of buoyancy on heat transfer to fluids flowing in vertical tubes under turbulent conditions, ed. J. Jackson and W. Hall. Vol. 2. 1979: Hemisphere Publishing Corporation.

25. Kao, M.-T., et al., *Heat transfer deterioration in a supercritical water channel.* Nuclear Engineering and Design, 2010. 240(10): p. 3321-3328.

APPENDIX

Table 5: Experimental Facility System Component Details

COMPONENT	MAKE/MODEL	SPECIFICATION
Magnetic Gear Pump	Micropump, Inc./200030 0512	
Electric Motor	Baldor-Reliance/IDNM3538	0.5 hp Maximum Output
Coriolis Flow Meter	Micro Motion/	-
Pre-heater	Tempco	5.5 kW Maximum Output
Power Supply	Magna-Power Electronics	5 kW Maximum Output
Water Chiller Unit	Advantage Engineering/M1-1.5A-21HFX	5.2 kW Capacity
High Performance Liquid Chromatography Pump	Chrom Tech, Inc./S10SNXP1	24 mL/min Maximum Fill Rate
Tube-in-Tube Heat Exchanger	Custom built for this experimental facility	-
Data Acquisition System	National Instruments	Varied
Pressure Transducer	Omega Engineering/PX309-3KG5V	0-3000 psig Range
Resistive Temperature Device (RTD)	Omega Engineering	